Inorganic Chemistry
Article

Inorg. Chem. **2010**, *49*, 6673–6689 **6673**
DOI: 10.1021/ic100712y

XeF_2 Coordination to a Halogen Center; Raman Spectra (n = 1, 2) and X-ray Crystal Structures (n = 2) of $[BrOF_2][AsF_6]\cdot nXeF_2$ and $[XOF_2][AsF_6]$ (X = Cl, Br)

David S. Brock,[†] Jonathan J. Casalis de Pury,[†] Hélène P. A. Mercier,[†] Gary J. Schrobilgen,*[,†] and Bernard Silvi[‡]

[†]*Department of Chemistry, McMaster University, Hamilton, Ontario, L8S 4M1, Canada, and*
[‡]*Laboratoire de Chimie Théorique, Université Pierre et Marie Curie, 4, place Jussieu, 75252 Paris cédex, France*

Received April 13, 2010

The syntheses and structural characterizations of the $[XOF_2][AsF_6]$ (X = Cl, Br) salts and the XeF_2 adduct-salts, $[BrOF_2][AsF_6]\cdot nXeF_2$ (n = 1, 2), are described. Although the $[XOF_2][AsF_6]$ salts have been known for some time, their crystal structures had not been reported until the present study. The crystal structure of $[BrOF_2][AsF_6]$ shows a positional disorder among the oxygen atom and the fluorine atoms. Both $ClOF_2^+$ and $BrOF_2^+$ have pseudo-octahedral coordination with a primary tripodal coordination sphere consisting of an oxygen atom and two fluorine atoms and a secondary coordination sphere consisting of three long contacts to fluorine atoms of different AsF_6^- anions. The low-temperature Raman spectra of $[XOF_2][AsF_6]$ have been assigned on the basis of the crystal structures and with the aid of quantum-chemical calculations using $[XOF_2][AsF_6]_3^{2-}$ as a model for the crystallographic environment of XOF_2^+. Several examples of XeF_2 coordinated through fluorine to transition metal centers are known, but no crystallographically characterized examples of XeF_2 coordinated to a nonmetal center other than xenon are known. The complex cation salts, $[BrOF_2][AsF_6]\cdot nXeF_2$ (n = 1, 2), were synthesized, and their Raman spectra have been assigned with the aid of quantum-chemical calculations. Although the structure of $[BrOF_2][AsF_6]\cdot 2XeF_2$ is similar to that of the recently reported krypton analogue, notable differences occur. The contact distances between bromine and the fluorine atoms of NgF_2 (Ng = Kr, Xe) are shorter in $[BrOF_2][AsF_6]\cdot 2XeF_2$ than in the KrF_2 analogue, which is attributed to the more polar natures of the Xe−F bonds. Unlike $[BrOF_2][AsF_6]\cdot 2KrF_2$, which has been shown in the prior study to be stable in HF solution at room temperature, $[BrOF_2][AsF_6]\cdot 2XeF_2$ enters into a dissociative equilibrium in which fluoride ion abstraction by $BrOF_2^+$ occurs to give $Xe_2F_3^+$ and $BrOF_3$. The ELF and QTAIM analyses of $[BrOF_2][AsF_6]_3^{2-}$ and $[BrOF_2][AsF_6]\cdot 2XeF_2$ were carried out and are compared with those of $[BrOF_2][AsF_6]\cdot 2KrF_2$ and for free $BrOF_2^+$ to better understand the effect of Br(V) coordination number on the localization domain of the Br(V) valence electron lone pair.

Introduction

Xenon difluoride behaves as a fluoride ion donor toward strong fluoride ion acceptors such as AsF_5, SbF_5, and BiF_5 forming XeF^+ and $Xe_2F_3^+$ salts.[1−5] Relatively few examples are known in which XeF_2 behaves as a coordinating ligand toward weaker Lewis acid centers. Coordination of a weak to moderate strength, oxidatively resistant Lewis acid to a fluorine atom of XeF_2 may also occur without "complete" fluoride ion transfer. A considerable number of metal cations satisfy these criteria, and their XeF_2 coordination complexes have been synthesized and structurally characterized, e.g., Li^+, Mg^{2+}, Ca^{2+}, Cu^{2+}, Zn^{2+}, Sr^{2+}, Ag^+, Cd^{2+}, Ba^{2+}, La^{3+}, Nd^{3+}, and Pb^{2+}.[6,7] Xenon difluoride coordination complexes with the neutral metal oxide tetrafluorides, WOF_4 and $MoOF_4$, have also been synthesized and characterized in the solid state by Raman spectroscopy and by solution ^{19}F and ^{129}Xe NMR spectroscopy.[8] A number of molecular addition compounds of XeF_2 are also known in which XeF_2 exhibits no tendency to coordinate. These are exemplified by $IF_5\cdot XeF_2$,[9] $XeF_4\cdot XeF_2$,[10] and $XeOF_4\cdot XeF_2$,[11] which show that the vibrational frequencies of XeF_2 and the Xe−F bond lengths are essentially unaffected relative to solid XeF_2.

Presently, the only examples known in which XeF_2 coordinates to a nonmetal center are $2XeF_2\cdot[XeF_5][AsF_6]$,

*Author to whom correspondence should be addressed. E-mail: schrobil@mcmaster.ca.

(1) Frlec, B.; Holloway, J. H. *J. Chem. Soc., A*. **1975**, 535–540.
(2) Gillespie, R. J.; Landa, B. *Inorg. Chem*. **1973**, *12*, 1383–1389.
(3) Sladky, F.; Bulliner, P. A.; Bartlett, N. *J. Chem. Soc., Dalton Trans*. **1969**, 2179–2188.
(4) Zalkin, A.; Ward, D. L.; Biagioni, R. N.; Templeton, D. H.; Bartlett, N. *Inorg. Chem*. **1978**, *17*, 1318–1322.
(5) Martin, D.; Gillespie, R. J.; Schrobilgen, G. J. *J. Chem. Soc., Dalton Trans*. **1980**, 1898–1903.
(6) Tavčar, G.; Tramšek, M.; Bunič, T.; Benkič, P.; Žemva, B. *J. Fluorine Chem*. **2004**, *125*, 1579–1584.
(7) Tramšek, M.; Žemva, B. *J. Fluorine Chem*. **2006**, *127*, 1275–1284.
(8) Holloway, J. H.; Schrobilgen, G. J. *Inorg. Chem*. **1980**, *19*, 2632–2640.
(9) Jones, G. R.; Burbank, R. D.; Bartlett, N. *Inorg. Chem*. **1970**, *9*, 2264–2268.
(10) Burns, J. H.; Ellison, R. D.; Levy, H. A. *Acta Crystallogr*. **1965**, *18*, 11–16.
(11) Bartlett, N.; Wechsberg, M. *Z. Anorg. Allg. Chem*. **1971**, *385*, 5–17.

Published on Web 06/18/2010

$XeF_2 \cdot [XeF_5][AsF_6]$, and $XeF_2 \cdot 2([XeF_5][AsF_6])$, where XeF_2 coordinates to the Xe(VI) atom of XeF_5^+,[12] and $[BrOF_2][AsF_6] \cdot XeF_2$, where XeF_2 coordinates to $BrOF_2^+$ through Br(V).[13] In both cases, XeF_2 coordinates end-on through fluorine to the electropositive atom of the cation. Although the XeF_5^+ adducts have been characterized by X-ray crystallography, $[BrOF_2][AsF_6] \cdot XeF_2$ has only been characterized by Raman spectroscopy and by solution ^{19}F and ^{129}Xe NMR spectroscopy. In a recent related study, $[BrOF_2][AsF_6] \cdot 2KrF_2$[14] has been synthesized and structurally characterized, showing that the KrF_2 molecules are each coordinated to Br(V) through a single fluorine bridge. The study suggested that the synthesis of $[BrOF_2][AsF_6] \cdot 2XeF_2$ should also be possible.

The present study describes the syntheses and structural characterizations of $[BrOF_2][AsF_6]$, $[ClOF_2][AsF_6]$, $[BrOF_2][AsF_6] \cdot XeF_2$, and $[BrOF_2][AsF_6] \cdot 2XeF_2$. The extension of this chemistry to the $ClOF_2^+$ analogue is also considered, as well as its Lewis acid behavior toward the less fluoro-basic and more strongly oxidizing XeF_4 molecule.

Results and Discussion

Syntheses of $[BrOF_2][AsF_6]$, $[BrOF_2][AsF_6] \cdot XeF_2$, and $[BrOF_2][AsF_6] \cdot 2XeF_2$. The progress of each reaction and the purities of all products were routinely monitored by recording the low-temperature Raman spectra of the solids at −150 °C.

Low-temperature solvolysis of $[XeOTeF_5][AsF_6]$ in liquid BrF_5 resulted in an XeF_2 adduct of $BrOF_2^+$ that also contained BrF_5 (eq 1).

$$[XeOTeF_5][AsF_6] + (n+1)BrF_5 \xrightarrow[20\ °C]{\text{neat}} [BrOF_2][AsF_6] \cdot XeF_2 \cdot nBrF_5 + TeF_6 \quad (1)$$

This compound was isolated as a very pale yellow powder upon removal of the bulk solvent under a dynamic vacuum at −52 to −50 °C. Continued pumping on the polycrystalline solid for several hours at −52 to −50 °C was shown by Raman spectroscopy (Table S1, Supporting Information) to result in the slow removal of BrF_5 from the crystal lattice, leaving behind $[BrOF_2][AsF_6] \cdot XeF_2$ as a white powder (eq 2). Further pumping at 0 °C for several hours resulted in slow removal of adducted XeF_2 (eq 3), forming $[BrOF_2][AsF_6]$ as a white powder.

$$[BrOF_2][AsF_6] \cdot nBrF_5 \cdot XeF_2 \xrightarrow[-52\ \text{to}\ -50\ °C]{\text{dynamic vac.}} [BrOF_2][AsF_6] \cdot XeF_2 + nBrF_5 \quad (2)$$

$$[BrOF_2][AsF_6] \cdot XeF_2 \xrightarrow[0\ °C]{\text{dynamic vac.}} [BrOF_2][AsF_6] + XeF_2 \quad (3)$$

The Raman spectrum of the product was in agreement with the previously reported spectrum;[15] however, contrary to the earlier report, samples of $[BrOF_2][AsF_6]$ that were left at room temperature overnight showed no signs of decomposition to Br_2^+ either visually or by Raman spectroscopy; i.e., the Br−Br stretching mode at 360 cm^{-1} was absent.[16] Hydrogen fluoride solutions of $[BrOF_2][AsF_6]$ were also warmed to 50 °C for several minutes followed by slow cooling to 22 °C over 24 h and showed no signs of decomposition.

The addition of anhydrous HF (aHF) to $[BrOF_2][AsF_6] \cdot XeF_2$ and dissolution at −20 °C resulted in a clear, colorless solution. Upon cooling to −78 °C, a white precipitate formed. The Raman spectrum of the solid under HF and the Raman spectrum recorded after HF had been removed under dynamic vacuum at −78 °C were identical and revealed that a mixture of $[BrOF_2][AsF_6] \cdot 2XeF_2$ and $[BrOF_2][AsF_6]$ had formed according to eq 4.

$$2[BrOF_2][AsF_6] \cdot XeF_2 \xrightarrow[-20\ °C]{HF} [BrOF_2][AsF_6] \cdot 2XeF_2 + [BrOF_2][AsF_6] \quad (4)$$

Under similar conditions, 1, 1.5, 2, and 3 equiv of XeF_2 were allowed to react with 1 equiv of $[BrOF_2][AsF_6]$ in HF solvent. Using 1 or 1.5 equiv of XeF_2, the Raman spectra of the isolated products showed them to be mixtures of $[BrOF_2][AsF_6]$ and $[BrOF_2][AsF_6] \cdot 2XeF_2$; with 2 equiv of XeF_2, the only product was $[BrOF_2][AsF_6] \cdot 2XeF_2$, and with 3 equiv, a mixture of $[BrOF_2][AsF_6] \cdot 2XeF_2$ and XeF_2 was obtained. No other adduct stoichiometries were detected.

Both $[BrOF_2][AsF_6] \cdot XeF_2$ and $[BrOF_2][AsF_6] \cdot 2XeF_2$ are kinetically stable for indefinite periods of time under anhydrous conditions at −78 °C. Concentrated (ca. 0.6 M) and dilute (ca. 0.3 M) HF solutions of both salts that had been warmed to 20 °C and then rapidly cooled to −78 °C showed only a mixture of $[BrOF_2][AsF_6]$ and $[BrOF_2][AsF_6] \cdot 2XeF_2$ as well as $[BrOF_2][AsF_6] \cdot 2XeF_2$, respectively, when their Raman spectra were recorded under frozen HF. Upon slow cooling of both concentrated solutions from 20 to −78 °C over several hours, two colorless layers formed as a result of the complex salting out of solution. Soon thereafter, the denser layer in both samples rapidly crystallized to give a mixture of $[BrOF_2][AsF_6]$ and $[BrOF_2][AsF_6] \cdot 2XeF_2$ as well as $[BrOF_2][AsF_6] \cdot 2XeF_2$, respectively. However, slow cooling of both dilute solutions from 20 to −78 °C over several hours resulted in predominantly the starting materials but also significant amounts of the fluoride ion abstraction products, $BrOF_3$ and $[Xe_2F_3][AsF_6]$, which formed according to eq 5.

$$BrOF_2^+{}_{(g)} + 2XeF_{2(g)} \longrightarrow Xe_2F_3^+{}_{(g)} + BrOF_{3(g)} \quad (5)$$

$$\Delta H^\circ_{rxn} = -44.3\text{kJ mol}^{-1};$$
$$\Delta G^\circ_{rxn} = +6.4\text{kJ mol}^{-1}; \text{MP2/aug-cc-pVTZ(-PP)}$$

$$\Delta H^\circ_{rxn} = -33.5\text{kJ mol}^{-1};$$
$$\Delta G^\circ_{rxn} = +4.8\text{kJ mol}^{-1}; \text{B3LYP/aug-cc-pVTZ(-PP)}$$

(12) Žemva, B.; Jesih, A.; Templeton, D. H.; Zalkin, A.; Cheetham, A. K.; Bartlett, N. *J. Am. Chem. Soc.* **1987**, *109*, 7420–7427.
(13) Keller, N.; Schrobilgen, G. J. *Inorg. Chem.* **1981**, *20*, 2118–2129.
(14) Brock, D. S.; Casalis de Pury, J. J.; Mercier, H. P. A.; Schrobilgen, G. J.; Silvi, B. *J. Am. Chem. Soc.* **2010**, *132*, 3533–3542.
(15) Bougon, R.; Huy, T. B.; Charpin, P.; Gillespie, R. J.; Spekkens, P. H. *J. Chem. Soc., Dalton Trans.* **1979**, *1*, 6–12.
(16) Gillespie, R. J.; Morton, M. J. *Chem. Commun.* **1968**, *24*, 1565–1567.

Both products were observed in the Raman spectrum, and $[Xe_2F_3][AsF_6]$ was also confirmed by several single-crystal unit cell determinations (trigonal phase[17]). The calculated Gibbs free energy for the major gas-phase decomposition pathway (eq 5) shows that the reaction is near equilibrium so that small changes in temperature, concentration, or solution conditions could account for an equilibrium shift that favors the formation of $Xe_2F_3^+$ and $BrOF_3$ in solution. The large positive ΔH_{rxn}° and ΔG_{rxn}° values associated with internal fluoride ion abstraction starting from the associated adduct (eq 6) relative to starting from its dissociated components (eq 5) suggests that the adduct is already at equilibrium with its dissociation products in HF solutions.

$$BrOF_2^+ \cdot 2XeF_{2(g)} \longrightarrow Xe_2F_3^+{}_{(g)} + BrOF_{3(g)} \qquad (6)$$

$$\Delta H_{rxn}^\circ = +158.0 \text{kJ mol}^{-1};$$

$$\Delta G_{rxn}^\circ = +124.6 \text{kJ mol}^{-1}; \text{B3LYP/aug-cc-pVTZ(-PP)}$$

^{129}Xe and ^{19}F NMR Spectroscopy. The ^{129}Xe and ^{19}F NMR spectra of $[BrOF_2][AsF_6]\cdot XeF_2$ had been previously recorded in BrF_5 solvent at −59 °C at an external field strength of 2.349 T (^{19}F, 94.1 MHz; ^{129}Xe, 27.86 MHz).[13] The study indicated that XeF_2 exchange was sufficiently fast on the NMR time scale to collapse the $^{19}F-{}^{19}F$ spin−spin couplings between the fluorine environments of coordinated XeF_2 ("XeF_2") and $BrOF_2^+$. In the present study, a sample of $[BrOF_2][AsF_6]\cdot XeF_2$ was dissolved in BrF_5 solvent, and the ^{129}Xe and ^{19}F NMR spectra were recorded at −60 °C at an external field strength of 11.744 T (^{19}F, 470.593 MHz; ^{129}Xe, 139.051 MHz) in an attempt to slow the chemical exchange rate sufficiently to observe the $^1J(^{19}F_t-{}^{129}Xe)$, $^1J(^{19}F_b-{}^{129}Xe)$, $^2J(^{19}F_t-{}^{19}F_b)$, $^2J(^{19}F_b-{}^{19}F_{Br})$, and $^3J(^{19}F_{Br}-{}^{129}Xe)$ couplings among the fluorine and xenon environments of "XeF_2" and $BrOF_2^+$. The ^{129}Xe and ^{19}F NMR spectra were similar to those reported previously [$\delta(^{19}F)$, 163.9 ppm, $\Delta\nu_{1/2}$ = 27 Hz; $\delta(^{129}Xe)$, −1358 ppm, $\Delta\nu_{1/2}$ = 38 Hz; $^1J(^{19}F-{}^{129}Xe)$ = 5680 Hz][13] with the exception of broader lines for "XeF_2" in the ^{19}F ($\Delta\nu_{1/2}$ = 1180 Hz) and ^{129}Xe ($\Delta\nu_{1/2}$ = 230 Hz) spectra, which indicated that "XeF_2" exchange was slowed, but not sufficiently to resolve any of the spin−spin couplings of the complex cation.

The ^{129}Xe and ^{19}F NMR spectra were also recorded for $[BrOF_2][AsF_6]\cdot 2XeF_2$ dissolved in BrF_5 solvent (−60 °C). The spectra were similar to those of the 1:1 adduct with single ^{19}F (−174.2 ppm) and ^{129}Xe (−1489 ppm) resonances for "XeF_2" but were more shielded than those of $[BrOF_2][AsF_6]\cdot XeF_2$ [$\delta(^{129}Xe)$, −1368 ppm; $\delta(^{19}F)$, −165.8 ppm] and less shielded than those of XeF_2 recorded in BrF_5 solvent [$\delta(^{129}Xe)$, −1708 ppm, −40 °C;[18] $\delta(^{19}F)$, −181.8 ppm, −20 °C[19]]. The ^{19}F resonance of "XeF_2" was also narrower in $[BrOF_2][AsF_6]\cdot 2XeF_2$ ($\Delta\nu_{1/2}$ = 320 Hz; $^1J(^{19}F-{}^{129}Xe)$ = 5660 Hz) when compared with that of $[BrOF_2][AsF_6]\cdot XeF_2$ ($\Delta\nu_{1/2}$ = 1180 Hz; $^1J(^{19}F-{}^{129}Xe)$ = 5678 Hz), indicating that "XeF_2" exchange was more rapid for $[BrOF_2][AsF_6]\cdot 2XeF_2$. The ^{129}Xe resonance of "XeF_2" was slightly broader in $[BrOF_2][AsF_6]\cdot 2XeF_2$ ($\Delta\nu_{1/2}$ = 310 Hz) when compared with that of $[BrOF_2][AsF_6]\cdot XeF_2$ ($\Delta\nu_{1/2}$ = 230 Hz). Exchange between coordinated "XeF_2" and free XeF_2 is expected to result in more pronounced broadening in the ^{129}Xe NMR spectrum than in the ^{19}F spectrum because of the greater frequency differences between complexed and free XeF_2 [$\delta(^{129}Xe, \text{"}XeF_2\text{"}) - \delta(^{129}Xe, XeF_2) \approx 9400$ Hz versus $\delta(^{19}F, \text{"}XeF_2\text{"}) - \delta(^{19}F, XeF_2) \approx 1500$ Hz].[18,19] However, the significant line narrowing that occurs in the ^{19}F NMR spectrum of "XeF_2" results from collapse of the $^2J(^{19}F_b-{}^{19}F_{Br})$ coupling, whereas collapse of the smaller $^3J(^{129}Xe-{}^{19}F_{Br})$ coupling in the ^{129}Xe NMR spectrum would not be expected to have a significant effect on the ^{129}Xe line width.

Attempted Syntheses of $[ClOF_2][AsF_6]\cdot 2XeF_2$ and XeF_4 Coordination Complexes of $[ClOF_2][AsF_6]$ and $[BrOF_2][AsF_6]$. An attempt to synthesize a XeF_4 adduct of $[BrOF_2][AsF_6]$ proved unsuccessful when an equimolar mixture of XeF_4 and $[BrOF_2][AsF_6]$ was dissolved at 50 °C in HF and cooled to 22 °C. A white precipitate formed, which was shown by Raman spectroscopy to be a mixture of the starting materials. This is not unexpected because the fluoride ion donor strength of XeF_4 is less than that of XeF_2.[20]

Attempts were made to synthesize XeF_2 and XeF_4 adducts of $[ClOF_2][AsF_6]$ in the hope that the chlorine analogue, by virtue of the greater electronegativity of chlorine, would prove to be a stronger Lewis acid. Mixtures of $XeF_2/[ClOF_2][AsF_6]$ and $XeF_4/[ClOF_2][AsF_6]$ dissolved in HF at −50 and 50 °C, respectively, were cooled to −78 °C, whereupon white solids precipitated. Raman spectra of both products were recorded under HF solvent and after the solvent had been removed under a dynamic vacuum at −78 °C. In both cases, the solids proved to be mixtures of the starting materials. In the case of the $XeF_2/[ClOF_2][AsF_6]$ system, warming of the HF solution to room temperature resulted in fluoride ion abstraction from XeF_2 by $ClOF_2^+$ to form $Xe_2F_3^+$ and $ClOF_3$ (eq 7).

$$[ClOF_2][AsF_6] + 2XeF_2 \xrightarrow[25\ ^\circ C]{HF} ClOF_3 + [Xe_2F_3][AsF_6] \qquad (7)$$

Evidence for fluoride ion abstraction is based on Raman spectroscopy of the frozen samples under HF and the unit cell dimensions of several $[Xe_2F_3][AsF_6]$ crystals (trigonal phase).[17] Raman spectroscopy confirmed the presence of $[Xe_2F_3][AsF_6]$, but $ClOF_3$ presumably remained in the frozen HF solvent phase and was too dilute to be observed in the Raman spectrum.

X-ray Crystallography. Summaries of the refinement results and other crystallographic information for $[BrOF_2][AsF_6]\cdot 2XeF_2$, $[BrOF_2][AsF_6]$, and $[ClOF_2][AsF_6]$ are

(17) Fir, B. A.; Gerken, M.; Pointner, B. E.; Mercier, H. P. A.; Dixon, D. A.; Schrobilgen, G. J. *J. Fluorine Chem.* **2000**, *105*, 159–167.

(18) Schrobilgen, G. J.; Holloway, J. H.; Granger, P.; Brevard, C. *Inorg. Chem.* **1978**, *17*, 980–987.

(19) Gillespie, R. J.; Schrobilgen, G. J. *Inorg. Chem.* **1976**, *15*, 22–31.

(20) $XeF_{2(g)} \rightarrow XeF^+_{(g)} + F^-_{(g)}$: ΔH_{rxn}° = +921.4 kJ mol^{-1}; ΔG_{rxn}° = +885.0 kJ mol^{-1}; MP2/(aug-)cc-pVTZ(-PP). $XeF_{4(g)} \rightarrow XeF_3^+{}_{(g)} + F^-_{(g)}$: ΔH_{rxn}° = +951.0 kJ mol^{-1}; ΔG_{rxn}° = +920.0 kJ mol^{-1}; MP2/(aug-)cc-pVTZ(-PP).

Table 1. Summary of Crystal Data and Refinement Results for $[BrOF_2][AsF_6]$, $[ClOF_2][AsF_6]$, and $[BrOF_2][AsF_6]\cdot 2XeF_2$

	$[BrOF_2][AsF_6]$	$[ClOF_2][AsF_6]$	$[BrOF_2][AsF_6]\cdot 2XeF_2$
space group	$P2_13$ (No. 198)	$Pna2_1$ (No. 33)	$P2_1/c$ (No. 14)
a (Å)	8.6144(3)	14.686(2)	5.9282(3)
b (Å)	8.6144(3)	5.2072(6)	13.9789(8)
c (Å)	8.6144(3)	8.1070(9)	15.3983(9)
β (deg)	90	90	111.859(2)
V (Å^3)	639.3(1)	620.0(2)	1184.3(1)
Z (molecules/unit cell)	4	4	4
mol. wt. (g mol^{-1})	1291.32	1113.48	2645.72
ρ_{calc} (g cm^{-3})	3.354	2.982	3.710
T (°C)	−173	−173	−173
μ (mm^{-1})	11.68	6.03	12.01
λ (Å)	0.71073	0.71073	0.71073
R_1[a]	0.0198	0.0304	0.0450
wR_2[b]	0.0370	0.0634	0.0932

[a] $R_1 = \sum||F_o| - |F_c||/\sum|F_o|$ for $I > 2\sigma(I)$. [b] wR_2 is defined as $\{\sum[w(F_o^2 - F_c^2)^2]/\sum w(F_o^2)^2\}^{1/2}$ for $I > 2\sigma(I)$.

Table 2. Selected Experimental and Calculated Geometrical Parameters for $[BrOF_2][AsF_6]\cdot 2XeF_2$

exptl[a]			PBE1-PBE[b]	B3LYP[b]
Bond Lengths (Å)				
Br(1)−O(1)	1.549(5)	Br(1)−O(1)	1.556	1.569
Br(1)−F(1)	1.736(4)	Br(1)−F(1)	1.733	1.758
Br(1)−F(2)	1.733(4)	Br(1)−F(2)	1.734	1.760
Br(1)---F(3)	2.306(4)	Br(1)---F(3)	2.303	2.323
Br(1)---F(5)	2.292(4)	Br(1)---F(5)	2.296	2.325
Br(1)---F(7)	2.610(4)	Br(1)---F(7)	2.579	2.561
Xe(1)−F(3)	2.052(4)	Xe(1)−F(3)	2.074	2.101
Xe(1)−F(4)	1.960(4)	Xe(1)−F(4)	1.948	1.971
Xe(2)−F(5)	2.053(4)	Xe(2)−F(5)	2.081	2.106
Xe(2)−F(6)	1.956(5)	Xe(2)−F(6)	1.945	1.968
Bond Angles (deg)				
F(1)−Br(1)−F(2)	89.6(2)	F(1)−Br(1)−F(2)	89.0	89.4
F(1)−Br(1)−O(1)	102.8(3)	F(1)−Br(1)−O(1)	101.8	101.8
F(1)−Br(1)---F(3)	84.8(2)	F(1)−Br(1)---F(3)	84.3	85.1
F(1)−Br(1)---F(5)	165.8(2)	F(1)−Br(1)---F(5)	166.5	166.1
F(1)−Br(1)---F(7)	84.9(2)	F(1)−Br(1)---F(7)	88.8	88.7
F(2)−Br(1)−O(1)	102.6(3)	F(2)−Br(1)−O(1)	100.0	100.2
F(2)−Br(1)---F(3)	163.2(2)	F(2)−Br(1)---F(3)	171.8	171.5
F(2)−Br(1)---F(5)	84.9(2)	F(2)−Br(1)---F(5)	82.4	83.2
F(2)−Br(1)---F(7)	81.0(2)	F(2)−Br(1)---F(7)	73.0	74.9
O(1)−Br(1)---F(3)	94.1(2)	O(1)−Br(1)---F(3)	86.1	87.3
O(1)−Br(1)---F(5)	91.2(2)	O(1)−Br(1)---F(5)	90.0	91.1
O(1)−Br(1)---F(7)	171.4(2)	O(1)−Br(1)---F(7)	167.3	168.5
F(3)−Xe(1)−F(4)	178.4(2)	F(3)−Xe(1)−F(4)	174.8	174.4
F(3)---Br(1)---F(5)	96.7(2)	F(3)---Br(1)---F(5)	103.2	100.8
F(3)---Br(1)---F(7)	82.7(2)	F(3)---Br(1)---F(7)	102.1	98.5
F(5)−Xe(2)−F(6)	179.8(2)	F(5)−Xe(2)−F(6)	175.9	176.3
F(5)---Br(1)---F(7)	81.3(2)	F(5)---Br(1)---F(7)	78.7	78.1
Br(1)---F(3)−Xe(1)	142.4(2)	Br(1)---F(3)−Xe(1)	149.5	151.0
Br(1)---F(5)−Xe(2)	134.1(2)	Br(1)---F(5)−Xe(2)	130.4	130.6
Br(1)---F(7)−As(1)	135.5(2)	Br(1)---F(7)−As(1)	116.6	123.3

[a] The atom labeling scheme corresponds to that used in Figure 1. [b] The aug-cc-pVTZ(-PP) basis set was used. The energy-minimized geometry was C_1. The atom labeling scheme corresponds to that used in Figure 2.

Table 3. Selected Geometrical Parameters for $[ClOF_2][AsF_6]$ (exptl) and $[ClOF_2][AsF_6]_3^{2-}$ (calcd)

exptl[a]			PBE1-PBE[b]	B3LYP[b]
Bond Lengths (Å)				
Cl(1)−O(1)	1.455(2)	Cl−O_1	1.409	1.421
Cl(1)−F(1)	1.522(2)	Cl−F_1	1.627	1.660
Cl(1)−F(2)	1.543(2)	Cl−F_2	1.627	1.659
Cl(1)---F(3)	2.476(2)	Cl---F_{3A}	2.304	2.317
Cl(1)---F(4A)	2.523(2)	Cl---$F_{3A'}$	2.305	2.317
Cl(1)---F(5B)	2.598(2)	Cl---F_{3B}	2.484	2.490
Bond Angles (deg)				
F(1)−Cl(1)−F(2)	98.7(1)	F_1−Cl−F_2	90.6	90.3
F(1)−Cl(1)−O(1)	105.5(1)	F_1−Cl−O_1	104.7	104.5
F(1)−Cl(1)---F(3)	163.3(1)	F_1−Cl---F_{3A}	163.9	163.7
F(1)−Cl(1)---F(4A)	91.5(1)	F_1−Cl---$F_{3A'}$	83.0	83.6
F(1)−Cl(1)---F(5B)	84.1(1)	F_1−Cl---F_{3B}	76.6	77.3
F(2)−Cl(1)−O(1)	104.2(1)	F_2−Cl−O_1	104.7	104.5
F(2)−Cl(1)---F(3)	84.7(1)	F_2−Cl---F_{3A}	82.4	83.1
F(2)−Cl(1)---F(4A)	157.7(1)	F_2−Cl---$F_{3A'}$	164.6	164.3
F(2)−Cl(1)---F(5B)	80.29(9)	F_2−Cl---F_{3B}	77.5	78.1
O(1)−Cl(1)---F(3)	89.3(1)	O_1−Cl---F_{3A}	91.1	91.6
O(1)−Cl(1)---F(4A)	92.1(1)	O_1−Cl---$F_{3A'}$	90.6	91.1
O(1)−Cl(1)---F(5B)	168.5(1)	O_1−Cl---F_{3B}	177.4	176.7
F(3)---Cl(1)---F(4A)	80.20(7)	F_{3A}---Cl---$F_{3A'}$	100.0	98.9
F(3)---Cl(1)---F(5B)	80.41(7)	F_{3A}---Cl---F_{3B}	87.7	86.7
F(4A)---Cl(1)---F(5B)	81.10(7)	$F_{3A'}$---Cl---F_{3B}	87.4	86.7
Cl(1)---F(3)−As(1)	141.2(1)	Cl---F_{3A}−As_A	131.2	132.1
Cl(1)---F(4A)−As(1A)	145.0(1)	Cl---$F_{3A'}$−$As_{A'}$	128.9	130.4
Cl(1)---F(5B)−As(1B)	137.7(1)	Cl---F_{3B}−As_B	135.0	137.4

[a] The atom labeling scheme corresponds to that used in Figure 3. [b] The Stutt Huzpolar 2 basis set was used. The energy-minimized geometry was C_1. The atom labeling scheme corresponds to that used in Figure S1 (Supporting Information).

provided in Table 1. Important bond lengths, bond angles, and contacts for $[BrOF_2][AsF_6]\cdot 2XeF_2$ and $[ClOF_2][AsF_6]$ are listed in Tables 2 and 3 and in Tables S2 and S3, Supporting Information.

(a) $[BrOF_2][AsF_6]\cdot 2XeF_2$. The compound, $[BrOF_2][AsF_6]\cdot 2XeF_2$, is isomorphous with $[BrOF_2][AsF_6]\cdot 2KrF_2$[14] and belongs to the $P2_1/c$ space group with a unit cell volume that is 87.7(3) Å^3 larger than that of the krypton analogue at the same temperature (−173 °C). The structure consists of well-separated $[BrOF_2][AsF_6]\cdot 2XeF_2$ units. The primary coordination sphere of the $BrOF_2^+$ cation is trigonal pyramidal, as observed in the KrF_2 analogue. A fluorine ligand of the AsF_6^- anion is coordinated trans to the oxygen atom, while the fluorine electron pair donor atoms of two XeF_2 molecules are coordinated trans to the fluorine atoms of $BrOF_2^+$ so that the coordination sphere around bromine is pseudo-octahedral (Figures 1 and 2), as observed in the KrF_2 analogue.[14]

The geometrical parameters of $BrOF_2^+$ in $[BrOF_2][AsF_6]\cdot 2XeF_2$ and $[BrOF_2][AsF_6]\cdot 2KrF_2$ are equal to within $\pm 3\sigma$. Although the Br−O bond length (1.549(5) Å) is very

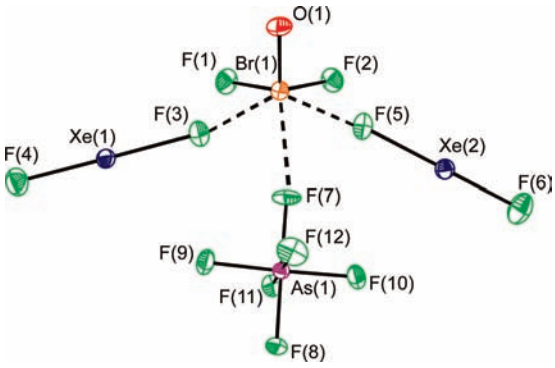

Figure 1. Structural unit in the X-ray crystal structure of $[BrOF_2][AsF_6]\cdot 2XeF_2$. Thermal ellipsoids are shown at the 50% probability level.

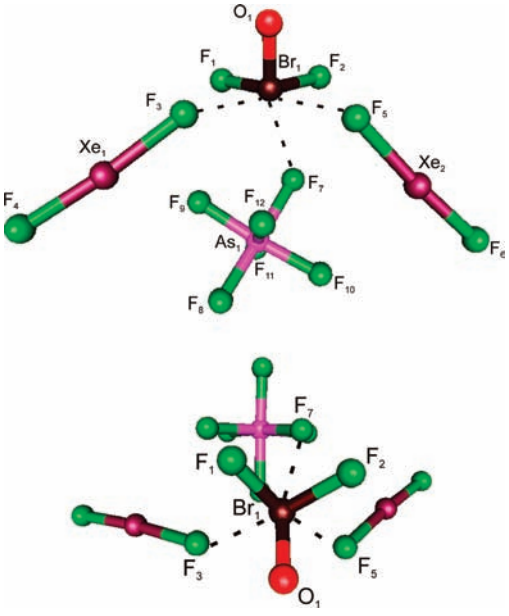

Figure 2. Calculated geometry (PBE1PBE/aug-cc-pVTZ(-PP)) of $[BrOF_2][AsF_6]\cdot 2XeF_2$ showing the pseudo-octahedral coordination around bromine(V).

similar to that of the KrF_2 analogue (1.564(5) Å),[14] it is significantly shorter than those of other Br(V) compounds, including the $BrOF_4^-$ anion in $[NO][BrOF_4]$ (1.575(3) Å),[21] $O_2Br-O-BrO_2$ (1.606 (12), 1.611(2), 1.613(2), 1.606(2) Å),[22] $O_2BrOTeF_5$ (1.595(4), 1.608(3) Å),[23] the parent molecule, $BrOF_3$, in $[NO_2][BrF_4]\cdot BrOF_3$ (1.569, 1.606 Å),[21] and the related BrO_2^+ cation in $[BrO_2][SbF_6]$ (1.595(2) Å).[24] The Br−O bond length is also shorter than the Se−O bond length of isoelectronic $SeOF_2$ (1.576 Å).[25] The Br−F bond lengths in $[BrOF_2][AsF_6]\cdot 2XeF_2$ (1.734(4), 1.736(4) Å) are intermediate with respect to the axial and equatorial Br−F bond lengths in the neutral parent molecule, $BrOF_3$ ($Br-F_{ax}$ = 1.820, 1.839, 1.822, 1.836 Å; $Br-F_{eq}$ = 1.725, 1.692 Å),[21] shorter than in the $BrOF_4^-$ anion (1.846(2), 1.912(2) Å),[21] and are essentially equal to those of the KrF_2 analogue, $[BrOF_2][AsF_6]\cdot 2KrF_2$ (1.727(4), 1.723(4) Å),[14] and the axial Br−F bond lengths of BrF_4^+ in $[BrF_4][Sb_2F_{11}]$ ($Br-F_{ax}$ = 1.728(3), 1.729(3) Å; $Br-F_{eq}$ = 1.664(3), 1.667(2) Å)[26] and the Se−F bond lengths in $SeOF_2$ (1.7255 Å).[25]

The fluorine bridge distances, Br---F, between the $BrOF_2^+$ cation and the coordinated XeF_2 molecules (Br---F(3), 2.306(4); Br---F(5), 2.292(4) Å) and between the $BrOF_2^+$ cation and the AsF_6^- anion (Br---F(7), 2.610(4) Å) are significantly less than the sum of the van der Waals radii of Br and F (3.32 Å).[27]

Coordination of XeF_2 to the $BrOF_2^+$ cation results in asymmetric Xe−F bond lengths, with the $Xe-F_b$ (2.052(4), 2.053(4) Å) and $Xe-F_t$ (1.960(4), 1.956(5) Å) bonds elongated and shortened, respectively, relative to those of solid XeF_2 at −173 °C (1.999(4) Å).[28] Such asymmetries have been previously observed for the KrF_2 analogue[14] and for XeF_2 terminally coordinated to metal centers.[6,7] The present $Xe-F_b$ and $Xe-F_t$ bond lengths are comparable to those in $[Ca(XeF_2)_5][PF_6]_2$,[29] $[Cd(XeF_2)_5][PF_6]_2$,[29] $[Cd(XeF_2)][BF_4]_2$,[30] $[Mg(XeF_2)_4][AsF_6]_2$,[31] $[Mg(XeF_2)_2][AsF_6]_2$,[31] and $[Ca_2(XeF_2)_9][AsF_6]_4$,[32] where the $Xe-F_b$ bonds range from 2.026(7) to 2.087(8) Å and the $Xe-F_t$ bonds range from 1.913(5) to 1.966(6) Å. The AsF_6^- anion in the present structure is a distorted octahedron in which the $As-F_b$ bridge bond is elongated relative to the other As−F bonds.

The XeF_2 ligands coordinate to bromine with Br(1)---F(3)−Xe(1) and Br(1)---F(5)−Xe(2) angles of 142.4(2)° and 134.1(2)°, respectively, which are bent as a result of steric repulsion between the two valence electron lone pairs of each bridging fluorine atom and their respective bridge bond pair domains. Both XeF_2 ligands are near-linear with F(3)−Xe(1)−F(4) and F(5)−Xe(2)−F(6) angles equal to 178.4(2)° and 179.8(2)°, respectively, consistent with other XeF_2 adducts.[6,7,29−32]

(b) $[BrOF_2][AsF_6]$. The unit cell of $[BrOF_2][AsF_6]$ contains four structural units and is in agreement with the previously reported cell parameters obtained from an earlier powder diffraction study.[15] The cubic space group, $P2/_13$, results in a 3-fold positional disorder around the bromine atom in which the oxygen and fluorine atoms of the trigonal pyramidal $BrOF_2^+$ cation are indistinguishable. The observed Br−O/F bond length (1.647(1) Å) is slightly shorter than the weighted average of the Br−O and Br−F bond lengths in $[BrOF_2][AsF_6]\cdot 2XeF_2$ (1.673(4) Å) (vide supra) and is consistent with the greater electronegativity of the bromine atom in $[BrOF_2][AsF_6]$ relative to that in $[BrOF_2][AsF_6]\cdot 2XeF_2$. Using a weighted apportioning of the calculated Br−O to Br−F bond length

(21) Ellern, A.; Boatz, J. A.; Christe, K. O.; Drews, T.; Seppelt, K. *Z. Anorg. Allg. Chem.* **2002**, *628*, 1991–1999.
(22) Leopold, D.; Seppelt, K. *Angew. Chem., Int. Ed. Engl.* **1994**, *33*, 975–976. *Angew. Chem.* **1994**, *106*, 1043−1044.
(23) Hwang, I.-C.; Kuschel, R.; Seppelt, K. *Z. Anorg. Allg. Chem.* **1997**, *623*, 379–383.
(24) Lehmann, J. F.; Riedel, S.; Schrobilgen, G. J. *Inorg. Chem.* **2008**, *47*, 8343–8356.
(25) Bowater, I. C.; Brown, R. D.; Burden, F. R. *J. Mol. Spectrosc.* **1968**, *28*, 461–470.
(26) Vij, A.; Tham, F. S.; Vij, V.; Wilson, W. W.; Christe, K. O. *Inorg. Chem.* **2002**, *41*, 6397–6403.
(27) Bondi, A. *J. Phys. Chem.* **1964**, *68*, 441–451.
(28) Lehmann, J. F. Ph. D. Thesis, McMaster University, Hamilton, ON, 2004.
(29) Bunič, T.; Tavčar, G.; Tramšek, M.; Žemva, B. *Inorg. Chem.* **2006**, *45*, 1038–1042.
(30) Tavčar, G.; Žemva, B. *Inorg. Chem.* **2005**, *44*, 1525–1529.
(31) Tramšek, M.; Benkič, T.; Žemva, B. *Inorg. Chem.* **2004**, *43*, 699–703.
(32) Tramšek, M.; Benkič, T.; Žemva, B. *Angew. Chem., Int. Ed.* **2004**, *43*, 3456–3458.

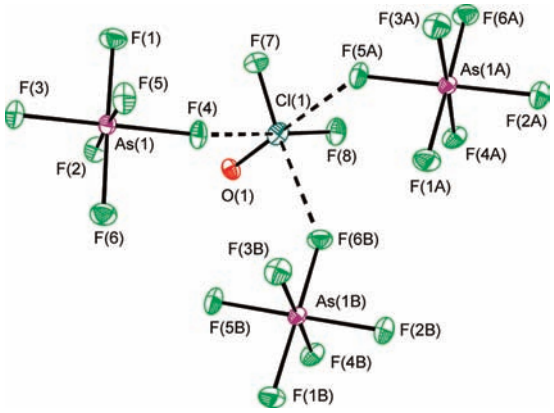

Figure 3. X-ray crystal structure of $[ClOF_2][AsF_6]$ showing the pseudo-octahedral coordination around chlorine(V). Thermal ellipsoids are shown at the 50% probability level.

ratio (0.891) obtained from the calculated structures of $[BrOF_2][AsF_6]_3^{2-}$ (see Computational Results), Br−O and Br−F bond lengths of 1.523 and 1.709 Å, respectively, may be assigned.

The bromine atom also makes three longer contacts with one fluorine atom of three different AsF_6^- anions, resulting in pseudo-octahedral coordination around the bromine atom. These contacts (2.506(1) Å) are significantly less than the sum of the van der Waals radii for Br and F (3.32 Å).

(c) $[ClOF_2][AsF_6]$. The unit cell contains four $[ClOF_2][AsF_6]$ structural units and differs from that deduced previously from an X-ray powder diffraction study which reported six structural units per unit cell.[33] The present study represents the first single-crystal X-ray structure determination of the $ClOF_2^+$ cation, and unlike the bromine analogue, the $ClOF_2^+$ cation is ordered.

The structure of $[ClOF_2][AsF_6]$ consists of a $ClOF_2^+$ cation which interacts by means of three nonequivalent short contacts with fluorine atoms from three AsF_6^- anions within the unit cell (Figure 3), providing the chlorine atom with a pseudo-octahedral coordination sphere similar to that of bromine in $[BrOF_2][AsF_6]$ and $[BrOF_2][AsF_6]\cdot 2XeF_2$ (vide supra). Three fluorine atoms of each AsF_6^- anion coordinate to three different $ClOF_2^+$ cations, generating a two-dimensional zigzag pattern of alternating $ClOF_2^+$ and AsF_6^- ions (Figure S2, Supporting Information), which is manifested in the crystal morphology, with the salt having a propensity to crystallize in very thin plates.

The Cl−O bond length (1.455(2) Å) is significantly longer than those of other Cl(V) species, including the ClO_2^+ cation in $[ClO_2][SbF_6]$ (1.385(5) Å),[24] $[ClO_2][RuF_6]$ (1.379(9) Å),[34] $[ClO_2][BF_4]$ (1.405(1), 1.408(1);[35] 1.397(2), 1.390(2)[36] Å), $[ClO_2][ClO_4]$ (1.406(2), 1.410(2) Å),[37] and $ClOF_3$ (1.405(3) Å; gas-phase electron diffraction)[38] and the estimated Cl−O bond length of $ClOF_2^+$ (1.41 Å) used to calculate its force constants.[39] Comparisons could not be made with the solid-state structure of $ClOF_3$ because the oxygen atom and the equatorial fluorine atom are positionally disordered. The Cl−O bond of $ClOF_2^+$ is also longer than the S−O bond in isoelectronic SOF_2 (1.412(1) Å)[40] but shorter than the Cl−O bond in the ClO_3^- anion of $[Na][ClO_3]$(1.502(3) Å).[41] This is in accord with the average lower formal Cl−O bond order of the ClO_3^- anion ($^5/_3$) compared to formal Cl−O and S−O bond orders of 2 for $ClOF_2^+$ and SOF_2. When compared with the calculated structure (see Computational Results), the experimental fluorine contact distance (Cl---F(5B)) opposite the oxygen atom is significantly shorter than the other Cl---F contact distances and is likely a result of crystal packing. This would account for lengthening of the Cl−O bond trans to it.

The Cl−F bond lengths (1.522(2), 1.543(2) Å) of $[ClOF_2][AsF_6]$ are comparable to the equatorial bond lengths of ClF_4^+ in $[ClF_4][SbF_6]$ (1.530(2) Å)[42] but are significantly shorter than the axial bonds of ClF_4^+ in $[ClF_4][SbF_6]$ (1.618(2) Å),[42] the axial and equatorial Cl−F bonds in gas-phase $ClOF_3$ ($Cl-F_{ax}$ = 1.713(3) Å; $Cl-F_{eq}$ = 1.603(4) Å),[38] and the S−F bonds in SOF_2 (1.585(1) Å),[40] as well as the estimated Cl−F bond length used to calculate the force constants of $ClOF_2^+$ (1.62 Å).[39]

The chlorine atom of $ClOF_2^+$ makes three additional long contacts with three neighboring AsF_6^- anions (Cl(1)---F(3) = 2.476(2) Å, Cl(1)---F(4A) = 2.523(2) Å, Cl(1)---F(5B) = 2.598(2) Å) that are substantially less than the sum of the van der Waals radii for Cl and F (3.22 Å). As a result, the AsF_6^- anions display distorted octahedral arrangements in which the three As−F bridge bonds are elongated and the bonds trans to the As−F bridge bonds are shortened.

Raman Spectroscopy. The low-temperature Raman spectra of solid $[BrOF_2][AsF_6]$, $[ClOF_2][AsF_6]$, $[BrOF_2][AsF_6]\cdot XeF_2$, and $[BrOF_2][AsF_6]\cdot 2XeF_2$ are shown in Figures 4−7. The observed and calculated frequencies and their assignments are listed in Tables 4−7 and Tables S4 and S5 (Supporting Information). The Raman spectra of $[BrOF_2][AsF_6]$ and $[ClOF_2][AsF_6]$ were assigned using the calculated $[BrOF_2][AsF_6]_3^{2-}$ and $[ClOF_2][AsF_6]_3^{2-}$ anions as models in which the cation coordinates by means of fluorine bridges to three different AsF_6^- anions, providing good approximations of the cation environments observed in their respective crystal structures (see Computational Results). The current work also shows that the previously reported Raman spectrum of $[BrOF_2][AsF_6]\cdot XeF_2$[13] contained small amounts of residual BrF_5 which was incorrectly assigned to $[BrOF_2][AsF_6]\cdot XeF_2$ (Table S1, Supporting Information).

The spectral assignments for $[BrOF_2][AsF_6]$, $[ClOF_2][AsF_6]$, $[BrOF_2][AsF_6]\cdot XeF_2$, and $[BrOF_2][AsF_6]\cdot 2XeF_2$ were made by comparison with the calculated frequencies

(33) Christe, K. O.; Schack, C. J.; Pilipovich, D. *Inorg. Chem.* **1972**, *11*, 2205–2208.
(34) Bougon, R.; Cicha, W. V.; Lance, M.; Meublat, L.; Nierlich, M.; Vigner, J. *Inorg. Chem.* **1991**, *30*, 102–109.
(35) Antipin, M. Y.; Ellern, A. M.; Sukhoverkhov, V. F.; Struchkov, Y. T.; Buslaev, Y. A. *Dokl. Akad. Nauk SSSR* **1987**, *293*, 1152–1155. *Dokl. Akad. SSSR, Engl.* **1987**, *293*, 354.
(36) Mallouk, T. E.; Rosenthal, G. L.; Müller, G.; Brusasco, R.; Bartlett, N. *Inorg. Chem.* **1984**, *23*, 3167–3173.
(37) Tobias, K. M.; Jansen, M. *Z. Anorg. Allg. Chem.* **1987**, *550*, 16–26.
(38) Oberhammer, H.; Christe, K. O. *Inorg. Chem.* **1982**, *21*, 273–275.
(39) Christe, K. O.; Curtis, E. C.; Schack, C. J. *Inorg. Chem.* **1972**, *11*, 2212–2215.
(40) Ferguson, R. C. *J. Am. Chem. Soc.* **1954**, *76*, 850–853.
(41) Burke-Laing, M. E.; Trueblood, K. N. *Acta Crystallogr., Sect. B* **1977**, *33*, 2698–2699.
(42) Christe, K. O.; Zhang, X.; Sheehy, J. A.; Bau, R. *J. Am. Chem. Soc.* **2001**, *123*, 6338–6348.

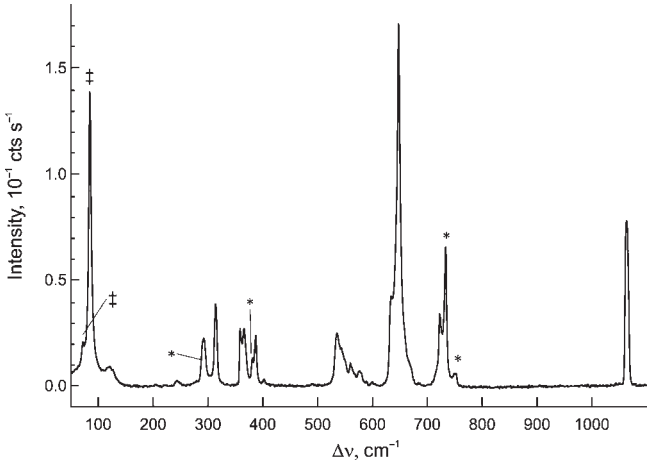

Figure 4. Raman spectrum of $[BrOF_2][AsF_6]$ recorded at −150 °C using 1064-nm excitation. Symbols denote FEP sample tube lines (∗) and instrumental artifacts (‡).

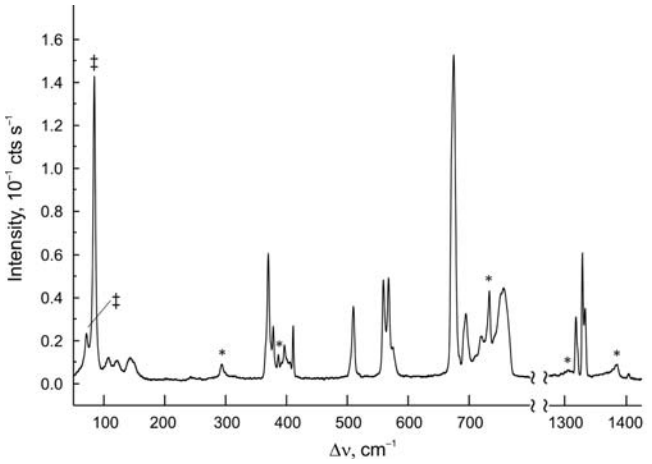

Figure 5. Raman spectrum of $[ClOF_2][AsF_6]$ recorded at −150 °C using 1064-nm excitation. Symbols denote FEP sample tube lines (∗) and instrumental artifacts (‡).

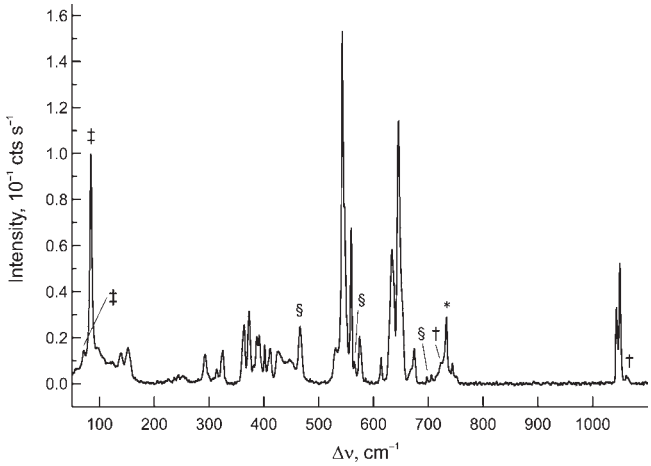

Figure 6. Raman spectrum of $[BrOF_2][AsF_6]\cdot XeF_2$ recorded at −150 °C using 1064-nm excitation. Symbols denote FEP sample tube lines (∗) and instrumental artifacts (‡), $[BrOF_2][AsF_6]$(†), and $[BrOF_2][AsF_6]\cdot 2XeF_2$(§).

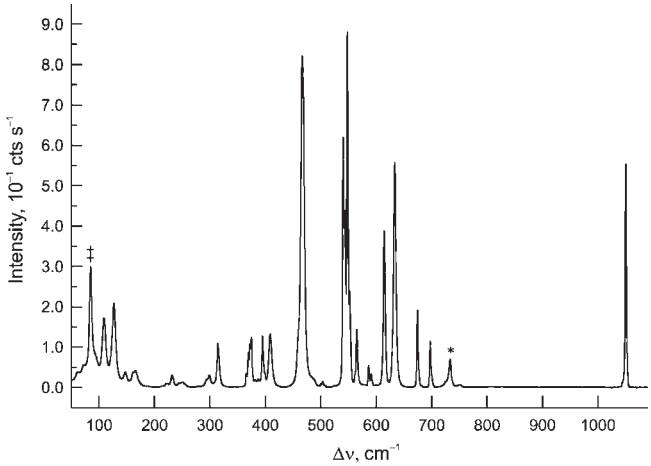

Figure 7. Raman spectrum of $[BrOF_2][AsF_6]\cdot 2XeF_2$ recorded at −150 °C using 1064-nm excitation. Symbols denote FEP sample tube lines (∗) and an instrumental artifact (‡).

and Raman intensities (Tables 4−7 and Tables S4 and S5, in the Supporting Information) of the energy-minimized geometries (Figure 2 and Figures S1, S3, and S4 in the Supporting Information) and for $[BrOF_2][AsF_6]\cdot 2XeF_2$ by comparison with $[BrOF_2][AsF_6]\cdot 2KrF_2$.[14] Vibrational frequencies calculated at the PBE1PBE and B3LYP (values in parentheses) levels of theory well reproduced the observed frequencies across the series of compounds. In each case, the AsF_6^- anion is distorted from its ideal octahedral geometry. The AsF_6^- anion, under O_h symmetry, has three Raman-active bands, $\nu_1(A_{1g})$, $\nu_2(E_g)$, and $\nu_5(T_{2g})$; two infrared-active bands, $\nu_3(T_{1u})$ and $\nu_4(T_{1u})$; and one inactive band, $\nu_6(T_{2u})$. In the present examples, the fluorine-bridged AsF_6^- anions are distorted, each with local C_1 symmetry, which results in a maximum of 15 Raman- and infrared-active bands. The bands that were observed in the Raman spectrum of AsF_6^- were assigned by comparison with other coordinated AsF_6^- anions having local C_1 or C_s symmetries.[43,44]

(a) $[BrOF_2][AsF_6]$. Although $[BrOF_2][AsF_6]$ has been previously characterized by Raman spectroscopy at room temperature,[15] the spectrum has been re-examined at low temperature to properly assess the effects of adduct formation on the $BrOF_2^+$ modes in $[BrOF_2][AsF_6]\cdot XeF_2$ and $[BrOF_2][AsF_6]\cdot 2XeF_2$. The experimental spectrum is in overall good agreement with the previously reported spectrum.

The cubic space group in which the crystal structure was solved implies that the anion and cation of $[BrOF_2][AsF_6]$ are situated on special positions with C_3 symmetry, thus imposing a 3-fold disorder on the cation. Consequently, the Raman spectrum was assigned on the basis of the calculated C_1 geometry. Under C_1 symmetry, all vibrational modes (27 A) of the $[BrOF_2][AsF_6]$ ion pair are predicted to be Raman- and infrared-active. Minor discrepancies are expected to arise between experimental and calculated modes involving the anion because the calculated model, $[BrOF_2][AsF_6]_3^{2-}$, is for a single cation coordinated to three anions (see Computational Results), whereas the crystal structure shows that

(43) Gerken, M.; Moran, M. D.; Mercier, H. P. A.; Pointner, B. E.; Schrobilgen, G. J.; Hoge, B.; Christe, K. O.; Boatz, J. A. *J. Am. Chem. Soc.* **2009**, *131*, 13474–13489.
(44) Smith, G. L.; Mercier, H. P. A.; Schrobilgen, G. J. *Inorg. Chem.* **2007**, *46*, 1369–1378.

Table 4. Selected Experimental and Calculated Vibrational Frequencies[a] for $[BrOF_2][AsF_6]$

exptl[b]			calcd[c]		assgnts
Raman[d,e]	infrared[d]	Raman[e,f]	PBE1PBE	B3LYP	$[BrOF_2][AsF_6]_3^{2-}$ (C_1)[g]
1059(50)	1055 m	1064(45)	1048(40)[78]	997(46)[72]	ν(BrO)
720(17)	730 sh	723(20)	687(26)[8]	665(25)[9]	$[\nu(As_AF_{6A}) + \nu(As_{A'}F_{6A'}) + \nu(As_BF_{6B})] + [\nu(BrF_1) + \nu(BrF_2)]$
			657(7)[35]	635(39)[<1] [h]	$[\nu(BrF_1) + \nu(BrF_2)] - [\nu(As_AF_{3A}) + \nu(As_AF_{4A}) + \nu(As_AF_{5A}) + \nu(As_AF_{6A}) + \nu(As_AF_{7A}) + \nu(As_AF_{8A})] + [\nu(As_{A'}F_{3A'}) + \nu(As_{A'}F_{4A'}) + \nu(As_{A'}F_{5A'}) + \nu(As_{A'}F_{6A'}) + \nu(As_{A'}F_{7A'}) + \nu(As_{A'}F_{8A'})] + [\nu(As_BF_{3B}) + \nu(As_BF_{4B}) + \nu(As_BF_{5B}) + \nu(As_BF_{6B}) + \nu(As_BF_{7B}) + \nu(As_BF_{8B})]_{small}$
	660 w	667 sh			
649(100)		647(100)	649(36)[176]	617(63)[81] [i]	$[\nu(BrF_1) + \nu(BrF_2)] + [\nu(As_AF_{8A}) + \nu(As_AF_{5A}) + \nu(As_AF_{3A}) + \nu(As_AF_{4A}) + \nu(As_AF_{7A}) - \nu(As_AF_{6A})] + [\nu(As_{A'}F_{8A'}) + \nu(As_{A'}F_{5A'}) + \nu(As_{A'}F_{3A'}) + \nu(As_{A'}F_{4A'}) + \nu(As_{A'}F_{7A'}) - \nu(As_{A'}F_{6A'})] - [\nu(As_{A'}F_{8A'}) + \nu(As_{A'}F_{5A'}) + \nu(As_{A'}F_{3A'}) - \nu(As_{A'}F_{6A'})]$
			648(46)[9]	629(3)[135] [j]	$[\nu(As_BF_{8B}) + \nu(As_BF_{5B}) + \nu(As_BF_{3B}) + \nu(As_BF_{4B}) + \nu(As_BF_{7B}) - \nu(As_BF_{6B})] + [\nu(BrF_1) + \nu(BrF_2)]$
634 sh	630 sh	634(25)	627(16)[191]	590(20)[159]	$[\nu(BrF_1) - \nu(BrF_2)]$
		549 sh	538(18)[25]	520(22)[29]	$[\nu(As_BF_{3B}) - \nu(BrF_{3B})] + \nu(As_BF_{6B})$
		543(10)	494(16)[146]	472(18)[150]	$[\nu(As_AF_{3A}) + \nu(As_{A'}F_{3A'}) - \nu(As_BF_{3B})] - [\nu(BrF_{3A}) + \nu(BrF_{3A'}) - \nu(BrF_{3B})]$
531(12)	535 m	535(14)	474(11)[224]	453(12)[218]	$[\nu(As_AF_{3A}) - \nu(As_{A'}F_{3A'})] + [\nu(BrF_{3A'}) - \nu(BrF_{3A})]$
398(1)	405 sh	403(2)	401(2)[122]	393(3)[106]	$[\delta(F_{4A}As_AF_{3A}) - \delta(F_{7A}As_AF_{6A}) + \rho_w(F_{8A}As_AF_{5A})] + [\delta(F_{4A'}As_{A'}F_{3A'}) - \delta(F_{7A'}As_{A'}F_{6A'}) + \rho_w(F_{8A'}As_{A'}F_{5A'})] + [\delta(F_{4B}As_BF_{3B}) - \delta(F_{7B}As_BF_{6B}) + \rho_w(F_{8B}As_BF_{5B})]_{small} + \delta(BrOF_1F_2)_{small}$
387(6)	385 ms	387(6)*	377(1)[143]	371(2)[158]	$[\delta(As_AF_{4A}F_{6A}F_{8A}) - \delta(As_AF_{3A}F_{5A}F_{7A})] - [\delta(As_{A'}F_{4A'}F_{6A'}F_{8A'}) - \delta(As_{A'}F_{3A'}F_{5A'}F_{7A'})] + \delta(OBrF_1)_{small}$
			377(<0.1)[1]	373(<0.1)[13]	$\delta(As_AF_{4A}F_{7A}F_{3A}F_{6A})_{o.o.p.} - \delta(As_{A'}F_{4A'}F_{7A'}F_{3A'}F_{6A'})_{o.o.p.}$
360(18)	355 sh	366(16)	359(3)[12]	346(3)[16]	$\delta(BrOF_1F_2)$
311(18)		314(23)	312(3)[90]	302(3)[79]	$\delta(OBrF_1)$
289(6)		292(6)*	283(<1)[24]	270(1)[21]	$\delta(F_1BrF_2)$
			162(<1)[33]	156(<1)[32]	$\rho_r(BrF_1F_2)$
119(4)		121(5)	153(<1)[33]	149(<1)[18]	$\rho_r(BrOF_1F_2)$
			127(<1)[3]	120(<1)[5]	$\rho_t(BrOF_1F_2)$

[a] Frequencies are given in cm^{-1}. [b] The abbreviations denote shoulder (sh), weak (w), medium (m), and medium-strong (ms). [c] The Stutt Huzpolar 2 basis set was used. Values in parentheses denote Raman intensities ($Å^4$ u^{-1}). Values in square brackets denote infrared intensities (km mol^{-1}). [d] From ref 15. [e] Values in parentheses denote relative Raman intensities. [f] The Raman spectrum was recorded in an FEP sample tube at −150 °C using 1064-nm excitation. An asterisk (*) indicates overlap with an FEP sample tube band; the relative Raman intensity does not include the FEP contribution. [g] Vibrational assignments were based on the modes at the PBE1PBE level. Only bands assigned to the $BrOF_2^+$ cation are given, and include those which exhibit coupling to the anion. The atom labeling scheme corresponds to that used in Figure S3 (Supporting Information). Complete assignments appear in Table S4 (Supporting Information). The abbreviations denote stretch (ν), bend (δ), rock (ρ_r), twist (ρ_t), and out-of-plane bend (o.o.p.). [h] $[\nu(As_AF_{8A}) + \nu(As_AF_{5A}) + \nu(As_AF_{3A}) + \nu(As_AF_{6A}) + \nu(As_AF_{4A}) + \nu(As_AF_{7A})] + [\nu(As_{A'}F_{8A'}) + \nu(As_{A'}F_{5A'}) + \nu(As_{A'}F_{3A'}) + \nu(As_{A'}F_{6A'}) + \nu(As_{A'}F_{4A'}) + \nu(As_{A'}F_{7A'})] + [\nu(As_BF_{8B}) + \nu(As_BF_{5B}) + \nu(As_BF_{3B}) + \nu(As_BF_{6B})]_{small} + [\nu(BrF_1) + \nu(BrF_2)]_{small}$. [i] $[\nu(BrF_1) + \nu(BrF_2)]$. [j] $[\nu(As_{A'}F_{8A'}) + \nu(As_{A'}F_{5A'}) + \nu(As_{A'}F_{3A'}) + \nu(As_{A'}F_{4A'}) + \nu(As_{A'}F_{7A'}) - \nu(As_{A'}F_{6A'})]$.

each AsF_6^- anion is also coordinated to three $BrOF_2^+$ cations.

In general, the cation bands are more intense than the anion bands, and little coupling occurs among their corresponding modes. The only significant exception is the in-phase Br−F stretching mode, $\nu(BrF_1) + \nu(BrF_2)$, which couples to As−F stretches of the anion (Table 4 and Table S4, Supporting Information) and results in several bands appearing at 647, 667, and 723 cm^{-1}. In contrast, the out-of-phase $\nu(BrF_1) - \nu(BrF_2)$ stretching band appearing at 634 cm^{-1} shows no coupling with the anion and is significantly less intense than the in-phase band, in agreement with the calculated intensities. The highest frequency band in the spectrum occurs at 1064 cm^{-1} and is assigned to ν(BrO), in agreement with the calculated value, 1048 (997) cm^{-1}. The Br---F_3 and As−F_3 stretches are coupled to one another and are assigned to the bands at 535, 543, and 549 cm^{-1}. The $OBrF_1F_2$ bending mode, $\delta(OBrF_1F_2)$, occurs at 366 cm^{-1}, and the remaining cation bending modes, $\delta(OBrF_1)$ and $\delta(F_1BrF_2)$, occur at 314 and 292 cm^{-1}, respectively.

(b) $[ClOF_2][AsF_6]$. The title compound has been previously characterized by Raman spectroscopy at room temperature.[39] However, a better-resolved, low-temperature spectrum is reported in the present work. The crystal structure of $[ClOF_2][AsF_6]$ has also made possible a more detailed analysis of the Raman spectrum which has been reassigned on the basis of a factor-group analysis.

All vibrational modes (27 A) of the $[ClOF_2][AsF_6]$ ion pair (C_1) are predicted to be Raman- and infrared-active. Although only 24 Raman bands were observed, several high-frequency stretching bands were split into two or three bands that cannot be accounted for by site symmetry lowering alone because correlation of the gas-phase ion-pair symmetry (C_1) to the crystal site symmetry (C_1) results in no additional band splittings. The additional bands therefore arise from vibrational coupling within the crystallographic unit cell. Correlation of the site symmetry to the centrosymmetric unit cell symmetry (C_{2v} with $Z = 4$) results in equal apportioning of the $4(3N - 6)$ vibrational modes among A_1, A_2, B_1, and B_2 components (Table S6, Supporting Information). The 27 vibrational bands split into A_1, A_2, B_1, and B_2 components, resulting in 108 coupled vibrational modes for $[ClOF_2][AsF_6]$ in its unit cell. The A_1, B_1, and B_2 components are Raman- and infrared-active, and the A_2 components are Raman-active. The appearance of only 24 Raman-active bands, instead of the predicted 108, implies that vibrational coupling within the unit cell is, for the most part, weak and cannot be resolved except for the highest frequency cation stretching modes.

When compared with the analogous bands in $[BrOF_2][AsF_6]$, the $ClOF_2^+$ bands are generally less intense than the AsF_6^- bands, in accordance with the lower polarizability of the Cl atom. Although the mode descriptions for $[ClOF_2][AsF_6]$ are very similar to those of the bromine analogue, there are small differences, including a general tendency for greater vibrational coupling between the cation and the anion modes in $[ClOF_2][AsF_6]$. The highest frequency bands at 1321, 1329, and 1333 cm^{-1} represent

Table 5. Selected Experimental and Calculated Vibrational Frequencies[a] for $[ClOF_2][AsF_6]$

exptl[b]			calcd[c]		assgnts
Raman[d]	infrared[d]	exptl[e,f]	PBE1PBE	B3LYP	$[ClOF_2][AsF_6]_3^{2-}$ (C_1)[g]
1333(2) 1320(1)	1331 ms 1319 mw	1333(21) 1329(39) 1321(10)	1303(41)[136]	1228(51)[126]	ν(ClO)
757(3)	750 br	757(26) br 752 (24) br	749(76)[299]	708(39)[386] [h]	$[\nu(ClF_1) + \nu(ClF_2)]$
		720(8)	729(14)[309]	702(3)[305] [i]	$[\nu(ClF_1) - \nu(ClF_2)] + [\nu(As_AF_{5A}) - \nu(As_AF_{8A})] - [\nu(As_{A'}F_{5A'}) - \nu(As_{A'}F_{8A'})] + [\nu(As_BF_{5B}) - \nu(As_BF_{8B})]$
		710(1)	716(6)[107]	691(17)[22]	$[\nu(As_AF_{5A}) - \nu(As_AF_{8A})] - [\nu(As_{A'}F_{5A'}) - \nu(As_{A'}F_{8A'})] + [\nu(As_{A'}F_{7A'}) - \nu(As_{A'}F_{4A'})] + [\nu(ClF_1) - \nu(ClF_2)]_{small}$
696(1)	695 vs	695(16) 692 sh	703(4)[40]	668(11)[12] [j]	$[\nu(As_AF_{4A}) - \nu(As_AF_{7A})] + [\nu(As_BF_{7B}) - \nu(As_BF_{4B})] + [\nu(As_BF_{5B}) - \nu(As_BF_{8B})] + [\nu(ClF_1) - \nu(ClF_2)]_{small}$
			700(4)[33]	680(15)[51] [k]	$[\nu(As_{A'}F_{4A'}) - \nu(As_{A'}F_{7A'})] + [\nu(As_BF_{7B}) - \nu(As_BF_{4B})] + [\nu(As_BF_{8B}) - \nu(As_BF_{5B})] + [\nu(ClF_1) - \nu(ClF_2)]_{small}$
		685(3)	667(6)[336]	641(17)[300] [l]	$[\nu(As_AF_{6A}) - \nu(As_{A'}F_{6A'})] + [\nu(ClF_1) - \nu(ClF_2)]_{small}$
563(3)	561 ms	568(31) 559(30)	552(14)[2]	533(19)[6]	$[\nu(As_BF_{3B}) + \nu(As_BF_{6B})] - [\nu(As_BF_{4B}) + \nu(As_BF_{7B})] - [\nu(As_BF_{5B}) + \nu(As_BF_{8B})]$
			525(17)[95]	501(24)[112]	$[\nu(As_AF_{3A}) + \nu(As_{A'}F_{3A'}) - \nu(As_BF_{3B})] - [\nu(ClF_{3A}) + \nu(ClF_{3A'}) - \nu(ClF_{3B})] + \delta(ClOF_1F_2)_{small}$
			507(14)[166]	484(18)[185]	$[\nu(As_AF_{3A}) - \nu(As_{A'}F_{3A'})] + [\nu(ClF_{3A'}) - \nu(ClF_{3A})]$
511(2)	509 ms	510(22)	476(4)[36]	452(2)[43]	$\delta(ClOF_1F_2) + [\nu(As_AF_{3A}) + \nu(As_{A'}F_{3A'})] - [\nu(ClF_{3A}) + \nu(ClF_{3A'})]_{small}$
406(2)	407 sh	411(16)	406(2)[8]	391(2)[40]	$\delta(OClF_1)$
		396(10) 392(5)	385(1)[74]	377(2)[39]	$\delta(F_1ClF_2) + \delta(As_BF_{4B}F_{7B}F_{8B}F_{5B})_{o.o.p.} - \delta(As_AF_{4A}F_{7A}F_{8A}F_{5A})_{o.o.p.} - \delta(As_{A'}F_{4A'}F_{7A'}F_{8A'}F_{5A'})_{o.o.p.}$
	388 s		370(<1)[141]	363(<1)[113]	$[\delta(As_AF_{4A}F_{6A}F_{8A}) - \delta(As_AF_{3A}F_{5A}F_{7A})] + [\delta(As_{A'}F_{3A'}F_{5A'}F_{7A'}) - \delta(As_{A'}F_{4A'}F_{6A'}F_{8A'})] + \delta(OClF_1)_{small}$
371(4)		370(39)	344(3)[26]	349(1)[<1]	$[\delta(F_{6B}As_BF_{8B}) + \delta(F_{3B}As_BF_{5B})] + \delta(F_1ClF_2)_{small}$
			340(2)[47]	332(3)[38]	$[\delta(F_{4A}As_AF_{6A}) + \delta(F_{3A}As_AF_{7A})] + [\delta(F_{4B}As_BF_{6B}) + \delta(F_{3B}As_BF_{7B})] + \delta(OClF_2)_{small}$

[a] Frequencies are given in cm^{-1}. [b] The abbreviations denote shoulder (sh), broad (br), medium-weak (mw), medium-strong (ms), strong, (s), and very strong (vs). [c] The Stutt Huzpolar 2 basis set was used. Values in parentheses denote Raman intensities ($Å^4\ u^{-1}$). Values in square brackets denote infrared intensities (km mol^{-1}). [d] From ref 39. [e] Values in parentheses denote relative Raman intensities. [f] The Raman spectrum was recorded in an FEP sample tube at −150 °C using 1064-nm excitation. Several weak bands were are also observed at 1065(2), 1045(4), and 1039(1) and are assigned to combination bands. [g] Vibrational assignments were based on the modes at the PBE1PBE level. Only bands assigned to the $ClOF_2^+$ cation are given and include those which exhibit coupling to the anion. The atom labeling scheme corresponds to that used in Figure S1 (Supporting Information). Complete assignments appear in Table S5 (Supporting Information). The abbreviations denote stretch (ν), bend (δ), and out-of-plane bend (o.o.p.). [h] $[\nu(ClF_1) + \nu(ClF_2)] + [\nu(As_AF_{8A}) - \nu(As_AF_{5A})] + [\nu(As_{A'}F_{8A'}) - \nu(As_{A'}F_{5A'})]$. [i] $[\nu(As_AF_{5A}) - \nu(As_AF_{8A})] - [\nu(As_{A'}F_{5A'}) - \nu(As_{A'}F_{8A'})] + [\nu(As_BF_{5B}) - \nu(As_BF_{8B})] + [\nu(ClF_1) - \nu(ClF_2)]_{small}$. [j] $[\nu(ClF_1) - \nu(ClF_2)] + [\nu(As_AF_{6A}) - \nu(As_{A'}F_{6A'})] - [\nu(As_BF_{5B}) - \nu(As_BF_{8B})]$. [k] $[\nu(As_BF_{4B}) - \nu(As_BF_{7B})] + [\nu(As_AF_{6A}) + \nu(As_{A'}F_{6A'})]_{small} + [\nu(ClF_1) + \nu(ClF_2)]_{small}$. [l] $[\nu(ClF_1) - \nu(ClF_2)] + [\nu(As_AF_{6A}) - \nu(As_{A'}F_{6A'})]$.

three of the four bands predicted for the factor-group split ν(ClO) mode which occur at higher frequencies than ν(BrO), in accordance with the greater electronegativity of chlorine and greater covalencies of the Cl−O and Cl−F bonds as well as the lower mass of chlorine. The coupling trends between the As−F and Br−F stretching modes of $[BrOF_2][AsF_6]$ are reversed in $[ClOF_2][AsF_6]$. The bands at 752 and 757 cm^{-1} are assigned to the in-phase $\nu(ClF_1) + \nu(ClF_2)$ mode and show no coupling to the anion modes, whereas the out-of-phase $\nu(ClF_1) - \nu(ClF_2)$ mode displays extensive coupling to As−F stretching modes with contributions observed at 685, 692, 695, 710, and 720 cm^{-1} with the major $\nu(ClF_1) - \nu(ClF_2)$ contribution assigned to the band at 720 cm^{-1}. The bands at 559 and 568 cm^{-1} arise from fluorine bridge stretches and are assigned to the different $\nu(AsF_3) - \nu(Cl\text{---}F_3)$ combinations of the three anions. The deformation modes of the cation are generally underestimated by the calculations and show significant coupling to the anion deformation modes. The mode having $\delta(OClF_1F_2)$ as its main contribution is coupled to AsF_6^- deformation modes and is assigned to the band at 510 cm^{-1}, which appears at a much higher frequency than the analogous band in $[BrOF_2][AsF_6]$. However, the latter mode, $\delta(OBrF_1F_2)$, is not coupled to any of the AsF_6^- deformation modes. The $\delta(OClF_1)$ and $\delta(F_1ClF_2)$ bending modes also appear at higher frequency than in $[BrOF_2][AsF_6]$ and contribute to the bands at 411 and 296, 392 cm^{-1}, respectively.

(c) $[BrOF_2][AsF_6]\cdot XeF_2$ and $[BrOF_2][AsF_6]\cdot 2XeF_2$. The current work has shown that the previously reported Raman spectrum[13] of $[BrOF_2][AsF_6]\cdot XeF_2$ contained residual BrF_5 solvent (Table S1, Supporting Information). A sample of pure $[BrOF_2][AsF_6]\cdot XeF_2$ was synthesized, and the spectrum was reassigned. The Raman spectrum of the related $[BrOF_2][AsF_6]\cdot 2XeF_2$ adduct has also been assigned.

Several modes in the $[BrOF_2][AsF_6]\cdot 2XeF_2$ spectrum are split into two components. The splittings cannot be accounted for by site symmetry lowering because correlation of the gas-phase adduct symmetry (C_1) to the crystal site symmetry (C_1) results in no additional band splittings. The splittings must therefore result from vibrational coupling within the crystallographic unit cell (C_{2v} with $Z = 4$). On the basis of a factor-group analysis (Table S7, Supporting Information), each Raman- and infrared-active band is predicted to be split into an A_g and a B_g component in the Raman spectrum and into an A_u and a B_u component in the infrared spectrum.

The most intense bands in the spectra of $[BrOF_2][AsF_6]\cdot XeF_2$ and $[BrOF_2][AsF_6]\cdot 2XeF_2$ are associated with the XeF_2 ligand modes, although they are not as intense as the KrF_2 ligand bands in $[BrOF_2][AsF_6]\cdot 2KrF_2$.[14] The interaction between the XeF_2 molecule and the $BrOF_2^+$ cation observed in the crystal structure renders the Xe−F bonds inequivalent for each XeF_2 molecule, giving rise to two bond types, $Xe-F_b$ and $Xe-F_t$. The higher frequency bands of $[BrOF_2][AsF_6]\cdot XeF_2$ at 531, 543, and 559 cm^{-1} are assigned to the factor-group split terminal $Xe-F_t$ stretch. Like the KrF_2 analogue, the occurrence of two $Xe-F_t$ bonds in the $[BrOF_2][AsF_6]\cdot 2XeF_2$ adduct gives rise to factor-group split in-phase (548 and 552 cm^{-1}) and out-of-phase

Table 6. Experimental and Calculated Vibrational Frequencies[a] for $[BrOF_2][AsF_6]\cdot XeF_2$

exptl[b]	calcd[c] PBE1PBE	calcd[c] B3LYP	assgnts $[BrOF_2][AsF_6]\cdot XeF_2$ (C_1)[d]	AsF_6^-
1050(25)[e]	1090(40)[57]	1020(44)[55]	ν(BrO)	
1043(22)				
752(3)	753(2)[197]	731(1)[192]	$\nu(AsF_5) - \nu(AsF_8)$	$\nu_3(T_{1u})$
744(7)	749(5)[137]	727(3)[135]	$\nu(AsF_7) - \nu(AsF_{10})$	
706(3)	745(8)[120]	724(12)[128]	$\nu(AsF_9)$	
651 sh	670(39)[94]	644(9)[73]	$\nu(BrF_1) + \nu(BrF_2)$	
646(63)[f]				
674(9)[e]	662(31)[76]	640(82)[79]	$\nu(AsF_5) + \nu(AsF_7) + \nu(AsF_{10}) + [\nu(BrF_1) + \nu(BrF_2)]_{small}$	$\nu_1(A_{1g})$
669(4)				
634(27)[e,f]	632(20)[163]	603(24)[160]	$\nu(BrF_1) - \nu(BrF_2)$	
559(45)	589(31)[159]	584(29)[181]	$\nu(XeF_9)$	
543(100)				
531(11)				
575(14)	573(3)[22]	564(3)[22]	$[\nu(AsF_5) + \nu(AsF_8)] - [\nu(AsF_7) + \nu(AsF_{10})]$	$\nu_2(E_g)$
447(8) br	463(36)[343]	472(58)[349]	$\nu(XeF_3) + [\nu(AsF_6) - \nu(Br\text{---}F_6)]_{small}$	
426(10) br				
	437(2)[18]	423(3)[22]	$\nu(AsF_6) + \nu(Br\text{---}F_6)$	
	419(2)[61]	407(2)[35]	$[\nu(AsF_6) - \nu(Br\text{---}F_6)] + \delta(F_6AsF_8) - \delta(F_5AsF_9) + \rho_w(F_7AsF_{10})$	
411(11)	389(1)[52]	378(<1)[53]	$\delta(OBrF_1F_2) + \delta(F_5AsF_{10}) - \delta(F_7AsF_8) + \rho_w(F_6AsF_9)$	$\nu_4(T_{1u})$
	385(2)[22]	374(2)[13]	$\delta(F_5AsF_7) - \delta(F_8AsF_{10}) + \rho_w(F_6AsF_9)$	
402(12)	375(2)[25]	365(1)[5]	$\delta(F_5AsF_7) + \delta(F_8AsF_{10}) + [\delta(OBrF_1F_2)]_{small}$	
392(14)	370(1)[60]	357(2)[38]	$\delta(OBrF_1F_2) + \delta(AsF_7F_8F_9)$	
387(7)[g]	354(1)[102]	340(1)[135]	$\delta(F_5AsF_6) - \delta(F_5AsF_9) + \delta(OBrF_1)$	$\nu_5(T_{2g})$
	343(<1)[3]	333(<1)[7]	$\delta(F_6AsF_7) + \delta(F_9AsF_{10})$	
373(19)[e]	313(5)[76]	301(4)[96]	$\rho_w(OBrF_2) + \rho_t(F_1BrF_2) + [\nu(AsF_6) - \nu(Br\text{---}F_6)]_{small}$	
364(17)				
325(10)	294(<1)[11]	276(<1)[10]	$\delta(F_1BrF_2)$	
	259(<1)[39]	251(<1)[50]	$\rho_w(F_7AsF_{10}) - \rho_w(F_6AsF_9) + \delta(F_8AsF_9)$	
293(8)[g]	244(<1)[21]	233(<1)[4]	$\rho_w(F_5AsF_8) - \rho_w(F_6AsF_9) + \delta(F_3XeF_4)_{i.p.}$	
	234(<1)[19]	231(<1)[8]	$\rho_w(F_5AsF_8) - \rho_w(F_6AsF_9) - \delta(F_3XeF_4)_{i.p.}$	
	221(<0.1)[1]	226(<0.1)[13]	$\rho_w(F_5AsF_8) - \rho_w(F_7AsF_{10})$	$\nu_6(T_{2u})$
244(3)	207(<1)[9]	213(<0.1)[2]	$\delta(F_3XeF_4)_{o.o.p.}$	
	159(<1)[9]	154(<1)[10]	$\rho_r(F_1BrF_2) + \rho_w(OBrF_2) + \rho_r(F_7AsF_8)$	
152(11)	151(<1)[3]	148(<1)[4]	$\rho_r(OBrF_2) + \rho_r(F_8AsF_9)_{small}$	
140(9)	139(1)[13]	133(1)[12]	$\rho_w(OBrF_1) + \rho_r(AsF_7F_8F_{10}) + \rho_r(F_3XeF_4)$	
	103(2)[3]	106(<1)[<1]	$\rho_t(F_3XeF_4) + \rho_r(OBrF_1F_2)$	
	79(1)[2]	82(3)[4]	$\rho_r(OBrF_1F_2) + \rho_r(F_3XeF_4)$	
	72(<1)[<1]	73(<1)[1]	deformation modes $[BrOF_2][AsF_6]\cdot XeF_2$	
	63(<1)[2]	66(<1)[2]		
	47(<1)[<1]	63(<1)[<1]		
	35(<1)[<1]	44(<0.1)[<1]		
	27(1)[<1]	40(<1)[<1]		
	14(<1)[<1]	25(<1)[<1]		
124(7)			lattice modes	
98(11)				

[a] Frequencies are given in cm^{-1}. [b] The Raman spectrum was recorded in an FEP sample tube at −150 °C using 1064-nm excitation. Values in parentheses denote relative Raman intensities. The abbreviations denote shoulder (sh) and broad (br). Several weak bands were observed and assigned to the $[BrOF_2][AsF_6]$ ion pair [1062(3), 723(2), 314(4) cm^{-1}] and to the $[BrOF_2][AsF_6]\cdot 2XeF_2$ adduct [698(2), 674(2), 614(7), 586(2), 565(7), 547(sh), 466(17), 408(sh), 314(4) cm^{-1}]; the relative intensities have been corrected for the overlap. [c] The aug-cc-pVTZ(-PP) basis set was used. Values in parentheses denote Raman intensities ($Å^4\ u^{-1}$), and values in square brackets denote infrared intensities (km mol^{-1}). [d] Vibrational assignments were based on the modes at the PBE1PBE level. The atom labeling scheme corresponds to that used in Figure S4 (Supporting Information). The abbreviations denote stretch (ν), bend (δ), rock (ρ_r), twist (ρ_t), wag (ρ_w), in-plane bend (i.p.), and out-of-plane bend (o.o.p.). [e] The band overlaps with a $[BrOF_2][AsF_6]\cdot 2XeF_2$ band; the relative intensity was corrected for overlap. [f] The band overlaps with a $[BrOF_2][AsF_6]$ band; the relative intensity was corrected for overlap. [g] The band overlaps with an FEP sample tube line; the relative intensity was corrected for overlap.

(540 and 543 cm^{-1}) bands, which are in good agreement with their respective calculated values, 604 (584) and 600 (578) cm^{-1}. The split band at 426 and 447 cm^{-1} in the 1:1 adduct primarily corresponds to the bridging fluorine stretch $\nu(XeF_b)$, with a small contribution from $\nu(AsF_6) - \nu(Br\text{---}F_6)$. A factor-group split band at 460 and 467 cm^{-1} and a band at 409 cm^{-1} are observed for the 2:1 adduct and are assigned to $\nu(XeF_b)$. However, unlike the $\nu(XeF_t)$ modes, the $\nu(XeF_b)$ modes are only weakly coupled with each other. This contrasts with the KrF_2 adduct,[14] where the $Kr-F_b$ stretches are more strongly coupled than the $Kr-F_t$ stretches. The present assignments for the XeF_2 modes are in agreement with those reported for XeF_2 homoleptically coordinated to metal cations,[6,7] where the higher-frequency bands range from 544 to 584 cm^{-1} and are assigned to $Xe-F_t$ stretching modes and the lower frequency bands range from 411 to 479 cm^{-1} and are assigned to $Xe-F_b$ stretching modes. The doubly degenerate Π_u bend of free XeF_2, δ(FXeF), which is infrared-active but Raman-inactive, splits into

Table 7. Experimental and Calculated Vibrational Frequencies[a] for $[BrOF_2][AsF_6]\cdot 2XeF_2$

exptl[b]	calcd[c]		assgnts	
	PBE1PBE	B3LYP	$[BrOF_2][AsF_6]\cdot 2XeF_2$ (C_1)[d]	AsF_6^-
1051(62) 1045(1)	1071(67)[71]	1022(77)[69]	$\nu(BrO)$	
701 sh 697(13)	744(6)[172] 727(3)[163] 721(<1)[232]	717(6)[167] 703(4)[158] 696(<1)[223]	$\nu(AsF_{11}) - \nu(AsF_{12})$ $\nu(AsF_8)$ $\nu(AsF_9) - \nu(AsF_{10})$	$\nu_3(T_{1u})$
675(21)	662(21)[68]	636(67)[52]	$\nu(AsF_7) + \nu(AsF_9) + \nu(AsF_{10}) + \nu(AsF_{12})$ [e]	$\nu_1(A_{1g})$
634(63)	678(62)[87]	642(36)[97]	$\nu(BrF_1) + \nu(BrF_2)$ [f]	
614(43)	646(29)[84]	609(41)[61]	$\nu(BrF_1) - \nu(BrF_2)$	
552(26) 548(100)	604(46)[81]	584(41)[94]	$\nu(Xe_1F_4) + \nu(Xe_2F_6)$	
543(49) 540(69)	600(25)[236]	578(22)[256]	$\nu(Xe_1F_4) - \nu(Xe_2F_6)$	
591(2) 586(5)	573(2)[5]	556(2)[3]	$[\nu(AsF_9) + \nu(AsF_{10})] - [\nu(AsF_{11}) + \nu(AsF_{12})]$	$\nu_2(E_g)$
565(15) 561 sh	535(7)[95]	511(23)[210]	$\nu(AsF_7) + [\nu(Xe_1F_3) - \nu(AsF_{12})]_{small}$	$\nu_2(E_g)$
467(93), br 460 sh	503(47)[218]	485(38)[156]	$\nu(Xe_1F_3) + [\nu(Xe_2F_5) - \nu(AsF_7)]_{small}$	
409(15), br	463(18)[364]	434(20)[325]	$\nu(Xe_2F_5) - \nu(Xe_1F_3)_{small}$	
400(4)	400(<1)[53] 395(<1)[27] 394(<1)[34]	390(<1)[42] 385(<1)[42] 383(<1)[25]	$\delta(F_9AsF_{12}) - \delta(F_{10}AsF_{11}) + \rho_w(F_7AsF_8)$ $\delta(F_8AsF_9) - \delta(F_7AsF_{10}) + \rho_w(F_{11}AsF_{12})$ $\delta(AsF_7F_9F_{11}) - \delta(AsF_8F_{10}F_{12})$	$\nu_4(T_{1u})$
395(15)	386(3)[119]	368(3)[99]	$\delta(OBrF_1F_2)$	
372 sh 366(3)	366(1)[<1] 361(1)[<1] 356(<1)[<1]	357(1)[<0.1] 352(2)[2] 345(<1)[<1]	$\delta(F_9AsF_{12}) + \delta(F_{10}AsF_{11})$ $\delta(F_7AsF_{12}) + \delta(F_8AsF_{11})$ $\delta(F_7AsF_9) + \delta(F_8AsF_{10})$	$\nu_5(T_{2g})$
375(13) 369(10)	338(4)[90]	322(4)[79]	$\rho_w(OBrF_2) + \rho_t(F_1BrF_2)$	
315(12)	305(<1)[6]	286(<1)[6]	$\delta(F_1BrF_2)$	
299(3)	270(<1)[67]	258(<1)[59]	$\delta(F_5Xe_2F_6)_{o.o.p.}$	
	248(<0.1)[8]	242(<1)[8]	$[\rho_w(F_9AsF_{10}) - \rho_w(F_7AsF_8)] - \delta(F_3Xe_1F_4)_{i.p.}$	
	240(<1)[15]	234(<1)[13]	$[\rho_w(F_9AsF_{10}) - \rho_w(F_7AsF_8)] + \delta(F_3Xe_1F_4)_{i.p.}$	
250(1)	238(<1)[<1]	228(<1)[1]	$\delta(F_5Xe_2F_6)_{i.p.}$	
	235(<1)[2]	226(<1)[9]	$\rho_w(F_{11}AsF_{12}) - \rho_w(F_7AsF_8) + \rho_w(F_9AsF_{10})$	$\nu_6(T_{2u})$
	229(<0.1)[<1]	222(<0.1)[<1]	$\rho_w(F_9AsF_{10}) - \rho_w(F_{11}AsF_{12}) + \rho_w(F_7AsF_8)$	$\nu_6(T_{2u})$
232(3)	216(<1)[18]	198(<1)[10]	$\delta(F_3Xe_1F_4)_{o.o.p.}$	
222(1)	181(1)[6]	175(2)[7]	$\rho_t(OBrF_1F_2) + [\rho_t(F_5Xe_2F_6) + \rho_t(F_3Xe_1F_4)]_{small}$	
166(4)	159(1)[18]	154(2)[19]	$\rho_t(F_5Xe_2F_6) + \rho_t(OBrF_1F_2)_{small}$	
161(3)	155(1)[4]	149(1)[2]	$\rho_t(OBrF_1) + \rho_t(F_5Xe_2F_6)$	
147(3)	129(1)[5]	130(2)[6]	$\rho_t(OBrF_1F_2) + \rho_r(F_3Xe_1F_4)$	
	116(2)[4]	108(<1)[4]	$\rho_t(OBrF_1F_2) - \rho_r(F_3Xe_1F_4)$	
	104(2)[16]	95(<1)[8]	$\rho_t(F_3Xe_1F_4) + \rho_t(OBrF_1F_2)_{small}$	
	101(<1)[4]	93(1)[4]	$\rho_t(F_5Xe_2F_6) + \rho_t(OBrF_1F_2)_{small}$	
	81(<1)[2]	73(1)[<1]	deformation modes $[BrOF_2][AsF_6]\cdot 2XeF_2$	
	68(<1)[<1]	63(1)[<1]		
	61(<1)[<1]	58(<1)[<1]		
	54(<1)[<1]	46(<1)[<1]		
	46(<1)[<1]	42(<1)[1]		
	43(<1)[1]	38(<1)[<1]		
	39(<1)[<1]	33(<0.1)[<1]		
	29(<1)[<1]	24(<1)[1]		
	21(<1)[<1]	10(1)[<1]		
127(22) 109(18) 91(9) 61(2)			lattice modes	

[a] Frequencies are given in cm^{-1}. [b] The Raman spectrum was recorded in an FEP sample tube at −150 °C using 1064-nm excitation. Values in parentheses denote relative Raman intensities. The abbreviations denote a shoulder (sh) and broad (br). [c] The aug-cc-pVTZ(-PP) basis set was used. Values in parentheses denote Raman intensities ($Å^4\ u^{-1}$). Values in square brackets denote infrared intensities ($km\ mol^{-1}$). [d] Vibrational assignments were based on the modes at the PBE1PBE level. The atom labeling scheme corresponds to that used in Figures 1 and 2.The abbreviations denote stretch (ν), bend (δ), rock (ρ_r), twist (ρ_t), wag (ρ_w), in-plane bend (i.p.), and out-of-plane bend (o.o.p.). [e] $\nu(BrF_1) + \nu(BrF_2)$ also contributes at B3LYP level. [f] $\nu(AsF_{13}) + \nu(AsF_{14}) + \nu(AsF_{10}) + \nu(AsF_9)$ also contributes at B3LYP level.

two components upon coordination, $\delta(F_tXeF_b)_{o.o.p.}$ and $\delta(F_tXeF_b)_{i.p.}$, where the bends are with respect to the plane containing the two XeF_2 molecules and the bromine atom and are both Raman- and infrared-active. Both components are shifted to higher frequencies relative to Π_u in the infrared spectrum of XeF_2 (213 cm^{-1}).[45] In the 1:1 adduct, the $\delta(F_tXeF_b)_{o.o.p.}$ mode is observed at 244 cm^{-1} and the $\delta(F_tXeF_b)_{i.p.}$ mode at 293 cm^{-1}. Similarly, in $[BrOF_2][AsF_6]\cdot 2XeF_2$, the two out-of-plane bending modes are observed at 232 and 299 cm^{-1}, and an in-plane bend is observed as a weak band at 250 cm^{-1}. The second in-plane bend is predicted by calculations to be even weaker than the aforementioned modes and was not observed.

The observed and calculated frequencies for the anion and cation of $[BrOF_2][AsF_6]\cdot 2XeF_2$ are similar to those observed and calculated for the KrF_2 analogue.[14] All three adducts, $[BrOF_2][AsF_6]\cdot 2KrF_2$,[14] $[BrOF_2][AsF_6]\cdot 2XeF_2$, and $[BrOF_2][AsF_6]\cdot XeF_2$, demonstrate that, upon adduct formation, the stretching frequencies of $BrOF_2^+$ shift to lower values. When a single XeF_2 molecule coordinates to $BrOF_2^+$, ν(BrO) is lowered with respect to the ν(BrO) of $[BrOF_2][AsF_6]$ (1064 cm^{-1}) and splits into two bands at 1043 and 1050 cm^{-1}. The addition of a second XeF_2 molecule does not result in significant frequency lowering, with the factor-group split Br−O stretching band occurring at 1045 and 1051 cm^{-1}. The opposite trend is observed for the Br−F stretching frequencies upon XeF_2 coordination. Coordination of XeF_2 in $[BrOF_2][AsF_6]\cdot XeF_2$ has little effect on $\nu(BrF_1) - \nu(BrF_2)$ and $\nu(BrF_1) + \nu(BrF_2)$, which are essentially unshifted at 634 and 646/651 cm^{-1}, respectively, relative to the Br−F stretching frequencies of $[BrOF_2][AsF_6]$ at 634 and 647 cm^{-1}. Coordination of a second XeF_2 molecule, however, results in low-frequency shifts of the out-of-phase and in-phase Br−F stretches to 614 and 634 cm^{-1}, respectively. The two modes are shifted to somewhat lower frequency when compared with the observed (625; 644 cm^{-1}) and calculated [652(612); 683(644) cm^{-1}] frequencies of $[BrOF_2][AsF_6]\cdot 2KrF_2$.[14] The trends in the cation stretching frequencies on going from KrF_2 to XeF_2 can be accounted for by considering the bromine coordination sphere. In both structures, the AsF_6^- anion is coordinated trans to the oxygen atom; hence their ν(BrO) stretching frequencies are similar. Because the NgF_2 ligands are coordinated trans to fluorine, the Br−F stretching modes are expected to experience a greater effect upon substitution. Because krypton is more electronegative, KrF_2 is a somewhat weaker fluoride ion donor than XeF_2,[46] which is manifested by shorter Br---F_b contacts in the crystal structure of $[BrOF_2][AsF_6]\cdot 2XeF_2$ (see X-ray Crystallography) relative to those of $[BrOF_2][AsF_6]\cdot 2KrF_2$.[14] More electron density is expected to transfer to bromine in the XeF_2 adduct, shifting the Br−F stretching modes to a lower frequency (vide supra). The cation deformation modes in $[BrOF_2][AsF_6]\cdot XeF_2$ and $[BrOF_2][AsF_6]\cdot 2XeF_2$ show little change upon XeF_2 coordination relative to those of $[BrOF_2][AsF_6]$. The $\delta(F_1BrF_2)$ bending mode occurs at 325 cm^{-1} for the 1:1 adduct and at 315 cm^{-1} for the 2:1 adduct. Similarly, the $\delta(OBrF_1F_2)$ bending mode is observed at 395 cm^{-1} in $[BrOF_2][AsF_6]\cdot 2XeF_2$ and is coupled to AsF_6^- bending modes in $[BrOF_2][AsF_6]\cdot XeF_2$, which appear at 392 and 411 cm^{-1}. When compared with the KrF_2 adduct, the cation deformation frequencies of $[BrOF_2][AsF_6]\cdot 2XeF_2$ are essentially the same as those of $[BrOF_2][AsF_6]\cdot 2KrF_2$ and are in good agreement with the calculated values.

Computational Results. The energy-minimized geometries of the ion pairs $[BrOF_2][AsF_6]_3^{2-}$ and $[ClOF_2][AsF_6]_3^{2-}$, and the adduct $[BrOF_2][AsF_6]\cdot 2XeF_2$, were optimized at the PBE1PBE and B3LYP levels starting from their crystallographic coordinates and C_1 symmetry. The 1:1 adduct, $[BrOF_2][AsF_6]\cdot XeF_2$, although lacking a crystal structure, was optimized starting from the crystallographic coordinates of $[BrOF_2][AsF_6]\cdot 2XeF_2$, with one molecule of XeF_2 removed. All four structures resulted in stationary points with all frequencies real. The PBE1PBE and B3LYP (B3LYP values are given in parentheses) results are summarized in Tables 2−7 and Tables S2−S5 and S8−S13 (Supporting Information) and Figure 2 and Figures S1, S3, and S4 (Supporting Information).

(a) Geometries. (i) $[BrOF_2][AsF_6]_3^{2-}$ and $[ClOF_2][AsF_6]_3^{2-}$. The crystal structures of $[BrOF_2][AsF_6]$ and $[ClOF_2][AsF_6]$ show that both cations coordinate to a fluorine atom from each of three different AsF_6^- anions (vide supra). Models were calculated reflecting the observed structures, i.e., one cation interacting with a single fluorine atom from each of three different AsF_6^- anions. Although a simplification, these models provide close approximations of the cation environments in their respective crystal structures and a means to study the effects of ion-pairing. There are, however, some disparities between the experimental and calculated Raman frequencies and intensities and their detailed mode descriptions. These primarily occur for the anion modes because they are only singly coordinated in the models, whereas they are coordinated to three cations in their crystal lattices.

For $[BrOF_2][AsF_6]_3^{2-}$, the calculated Br−O bond length is 1.568 (1.580) Å and the Br−F bond lengths are 1.755 (1.779) Å. The weighted average bond length, 1.693 Å, is slightly greater than the experimental bond length in the disordered $BrOF_2^+$ cation (1.647(1) Å, see X-ray Crystallography). The fluorine atoms are bent away from the oxygen atom in $[BrOF_2][AsF_6]_3^{2-}$, with O−Br−F_1 and O−Br−F_2 angles of 101.1 (101.0)° and 101.1 (100.9)°, respectively, and an F_1−Br−F_2 angle of 89.2 (89.3)° giving an average angle of 97.1 (97.1)°. The average angle is slightly less than the F/O−Br−O/F angle in the disordered crystal structure of $[BrOF_2][AsF_6]$ (99.89(6)°). The three contact distances are 2.306 (2.328), 2.306 (2.327), and 2.481 (2.503) Å with the contact trans to the oxygen atom being the longest, in agreement with the experimental results. All contacts are significantly less than the sum of the bromine and fluorine van der Waals radii (3.32).[27]

The VSEPR[47] model of molecular geometry predicts that substitution of bromine by chlorine should result in a more localized valence electron lone pair domain on chlorine,

(45) Agron, P. A.; Begun, G. M.; Levy, H. A.; Mason, A. A.; Jones, C. G.; Smith, D. F. *Science* **1963**, *139*, 842–844.

(46) Gas-phase fluoride ion donor strengths ($NgF_{2(g)} \rightarrow NgF^+_{(g)} + F^+_{(g)}$, given in kJ mol^{-1}) for XeF_2 (ΔH = 921.4, 922.3; ΔG = 885.0, 888.9) and for KrF_2 (ΔH = 951.8, 953.6; ΔG = 917.4, 919.4) were calculated at the MP2 and B3LYP levels of theory, respectively, using the aug-cc-pVTZ(-PP) basis set.

(47) Gillespie, R. J.; Hargittai, I. In *The VSEPR Model of Molecular Geometry*; Allyn and Bacon: Boston, MA, 1991; pp 154−155.

resulting in smaller O−Cl−F and F−Cl−F angles. Instead, small increases in the O−Cl−F_1, O−Cl−F_2, and F−Cl−F angles to 104.7 (104.5)°, 104.7 (104.5)°, and 90.6 (90.3)° are observed relative to those of the bromine analogue, which are likely a consequence of the shorter Cl−O bond length [1.409 (1.421) Å] and Cl−F bond lengths [1.627 (1.660) and 1.627 (1.659) Å]. These differences can be accounted for by the ligand close packing model.[48] As expected, the three Cl---F_b contacts, 2.304 (2.317), 2.305 (2.317), and 2.484 (2.490) Å, in [$ClOF_2$][AsF_6] are also shorter than in the bromine analogue and are significantly less than the sum of the chlorine and fluorine van der Waals radii (3.22).[27] As is the case for the calculated geometry of the bromine analogue and in the crystal structure of [$ClOF_2$][AsF_6], the longest X---F contact is trans to the oxygen atom.

In both [$BrOF_2$][AsF_6] and [$ClOF_2$][AsF_6], the AsF_6^- anion is distorted from its ideal octahedral geometry with the As−F_b bond lengths ranging from 1.785 (1.795) to 1.822 (1.834) Å in the $BrOF_2^+$ salt and from 1.772 (1.782) to 1.798 (1.811) Å in the $ClOF_2^+$ salt. Consequently, the As−F_t bond lengths are shorter, ranging from 1.728 (1.736) to 1.741 (1.750) Å in the [$BrOF_2$][AsF_6] and from 1.730 (1.738) to 1.744 (1.752) Å in [$ClOF_2$][AsF_6].

(ii) [$BrOF_2$][AsF_6]·XeF_2. Although an experimental structure is unavailable for [$BrOF_2$][AsF_6]·XeF_2, the Br(V) atom is expected to complete a pseudo-octahedral coordination sphere by making contacts with two different AsF_6^- anions in the crystal lattice. A simplified ion-pair model involving a single anion was calculated starting from the crystallographic coordinates of [$BrOF_2$][AsF_6]·$2XeF_2$ with one XeF_2 molecule removed. The energy-minimized geometry optimized to C_1 symmetry. The bromine center displays a pseudo-octahedral geometry when the contacts to the bridging fluorine atom of XeF_2 and the two fluorine atoms of the AsF_6^- anion are taken into account. When compared with [$BrOF_2$][AsF_6], the cation is relatively unaffected by the introduction of one molecule of XeF_2 into the coordination sphere of Br(V), resulting in a Br−O bond length of 1.554 (1.567) Å and Br−F bond lengths of 1.730 (1.753) and 1.752 (1.777) Å. There is also little change in the O−Br−F_1 (102.8 (102.5)°), O−Br−F_2 (100.5 (100.5)°), and F_1−Br−F_2 (89.0 (89.4)°) angles upon coordination. The three contact distances to the cation are, however, significantly affected by XeF_2 coordination. The longest contact to F_5 of the AsF_6^- anion remains trans to the oxygen atom in [$BrOF_2$][AsF_6]·XeF_2 but is lengthened (2.708 (2.729) Å) relative to [$BrOF_2$][AsF_6]$_3^{2-}$ (2.481 (2.503) Å). The Br---F contact with XeF_2, which is trans to a fluorine atom, is 2.369 (2.397) Å and is slightly longer than in the 2:1 adduct (2.303 (2.323); 2.296 (2.325) Å). The shortest contact to bromine (2.162 (2.178) Å) is with F_6 of the AsF_6^- anion, which is trans to the other fluorine atom of $BrOF_2^+$ and shorter than in [$BrOF_2$][AsF_6]$_3^{2-}$ (2.306 (2.327)Å).

The coordinated XeF_2 ligand is distorted relative to free XeF_2 (1.986 (2.010) Å) with the Xe−F_b bond elongated (2.068 (2.083) Å) and the Xe−F_t bond length shortened (1.948 (1.976) Å) by equal amounts. As observed for the AsF_6^- anion in [$BrOF_2$][AsF_6], the As−F_b bonds of the anion are elongated relative to the As−F_t bonds.

(iii) [$BrOF_2$][AsF_6]·$2XeF_2$. The geometry of [$BrOF_2$][AsF_6]·$2XeF_2$ optimized to C_1 symmetry, providing a good approximation of the structural unit in the X-ray crystal structure. The calculations predict very little effect on the cation when XeF_2 is substituted for KrF_2.[14] The Br−O bond length remains unchanged (1.556 (1.569) Å), and the Br−F bond lengths are only slightly lengthened (1.733 (1.758) and 1.734 (1.760) Å) relative to [$BrOF_2$][AsF_6]·$2KrF_2$.[14] This behavior is also observed experimentally where both the Br−O (1.549(5) Å) and Br−F (1.736(4), 1.733(4) Å) bond lengths are equal to within $\pm 3\sigma$ for the XeF_2 and KrF_2 adducts.[14] Similarly, the O−Br−F_1 (101.8 (101.8)°), O−Br−F_2 (100.0 (100.2)°), and F−Br−F (89.0 (89.4)°) angles in the calculated [$BrOF_2$][AsF_6]·$2XeF_2$ structure are essentially unaffected by XeF_2 coordination, which is also observed in the crystal structures. In addition, the longest contact to F_7 of AsF_6^- (2.579 (2.561) Å), which is trans to the oxygen atom, is predicted to be unchanged. However, the two other contact distances to F_3 [2.303 (2.323) Å] and to F_5 [2.296 (2.325) Å] of the XeF_2 ligands are predicted to be shorter than in the KrF_2 adduct.[14] Shortening of these contacts upon coordination of XeF_2 is also observed in the crystal structures and is attributed to the greater fluoride ion donor strength of XeF_2 (see Raman Spectroscopy).

The XeF_2 ligands are also well modeled by the calculations. The calculated Xe−F_t bond lengths (1.948 (1.971), 1.945 (1.968) Å) are shorter than the Xe−F_b bond lengths (2.074 (2.101) Å, 2.081 (2.106) Å), in agreement with experimental values (1.960(4), 1.956(5), and 2.052(4), 2.053(4) Å, respectively). The calculated F−Xe−F angles are slightly bent (174.8 (174.4) and 175.9 (176.3)°), as observed in the crystal structure (178.4(2), 179.8(2)°).

The bond lengths and bond angles are also well reproduced for the AsF_6^- anion and are almost identical to those predicted for the AsF_6^- anion in [$BrOF_2$][AsF_6]·$2KrF_2$[14] where the AsF_6^- environment is very similar. The ideal octahedral anion symmetry is distorted by fluorine bridging to the cation. The calculated As−F_b bridge bond length is 1.789 (1.812) Å, which is elongated relative to the remaining As−F bonds (1.706 (1.720)−1.758 (1.771) Å), as observed in the crystal structure.

(b) Natural Bond Orbital (NBO) Analyses. The NBO[49−52] analyses were carried out for the PBE1PBE- and B3LYP-optimized gas-phase geometries of [$ClOF_2$][AsF_6]$_3^{2-}$, [$BrOF_2$][AsF_6]$_3^{2-}$, [$BrOF_2$][AsF_6]·$2XeF_2$, AsF_6^-, and XeF_2 with the results given in Tables S11−S13 (Supporting Information). The PBE1PBE and B3LYP results are similar across the series of compounds with the exception of the AsF_6^- anion, where the PBE1PBE valencies and bond orders are lower than the B3LYP values; only

(48) Gillespie, R. J.; Robinson, E. A.; Pilmé, J. *Chem.—Eur. J.* **2010**, *16*, 3663–3675.

(49) Reed, A. E.; Weinstock, R. B.; Weinhold, F. *J. Chem. Phys.* **1985**, *83*, 735–746.

(50) Reed, A. E.; Curtiss, L. A.; Weinhold, F. *Chem. Rev.* **1998**, *88*, 899–926.

(51) Glendening, E. D.; Reed, A. E.; Carpenter, J. E.; Weinhold, F. *NBO*, version 3.1; Gaussian Inc.: Pittsburgh, PA, 1990.

(52) Glendening, E. D.; Badenhoop, J. K.; Reed, A. E.; Carpenter, J. E.; Bohmann, C. M.; Morales, C. M.; Weinhold, F. *NBO*, version 5.0; Theoretical Chemistry Institute, University of Wisconsin: Madison, WI, 2001.

the B3LYP results are referred to in the ensuing discussion.

(i) $[ClOF_2][AsF_6]_3^{2-}$ and $[BrOF_2][AsF_6]_3^{2-}$. The positive charge is localized on the central halogen atoms of the $ClOF_2^+$ and $BrOF_2^+$ cations of $[ClOF_2][AsF_6]_3^{2-}$ and $[BrOF_2][AsF_6]_3^{2-}$ and is approximately half the halogen charge in the fully ionic model. The bromine charge (2.36) is higher than that of chlorine (2.09), which is in accordance with the lower electronegativity of bromine. The higher bromine charge is also accompanied by an increase in negative charge of the ligands that is primarily dispersed onto the oxygen atom, with the charge increased by −0.16, and onto the fluorine atoms, with the charge increased by −0.09 for each fluorine atom. The aforementioned charge differences are reflected in the greater X−O and X−F valencies and bond orders and are consistent with the greater covalent characters of the Cl−O and Cl−F bonds. Of the possible valence bond descriptions for XOF_2^+ (structures I−IV), the charges, valencies, and bond orders are best described for $ClOF_2^+$ by structure IV, with an almost equal contribution from structure I, and a minor contribution from structure III. In contrast, the NBO parameters of $BrOF_2^+$ are best represented by a much greater contribution from structure IV and minor contributions from structures I and III.

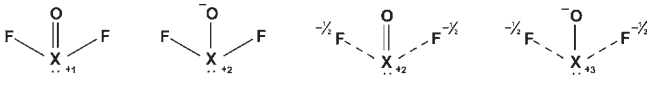

I II III IV

The net positive charges for the $ClOF_2^+$ (0.83) and $BrOF_2^+$ (0.76) cations are indicative of similar charge transfers of ca. 0.17 and 0.24*e*, respectively, from the anions to the cation in their ion pairs. Anion−cation charge transfers in $[ClOF_2][AsF_6]_3^{2-}$ and in $[BrOF_2][AsF_6]_3^{2-}$ are also consistent with the Cl---F (0.054, 0.55, 0.024) and Br---F (0.101, 0.101, 0.056) bridge bond orders and polarization of the negative charge on the anion toward the halogen atom.

(ii) $[BrOF_2][AsF_6]\cdot 2XeF_2$. The XeF_2 ligands are polarized toward bromine with ca. 0.08*e* transferred from each XeF_2 molecule. The Br---F bond orders of the bridging fluorines are 0.08, indicating that the Br---F interaction is weakly covalent. The polarization trend, magnitude of charge transfer, and the bond orders are very similar to those observed for $[BrOF_2][AsF_6]\cdot 2KrF_2$.[14] In fact, coordination of either XeF_2 or KrF_2 has no significant effect on the net charge of the cation (0.78 *e*, $[BrOF_2][AsF_6]\cdot 2XeF_2$; 0.80 *e*, $[BrOF_2][AsF_6]\cdot 2KrF_2$[14]).

Instead of the cation experiencing the effects of the negative charge transfer from the XeF_2 and KrF_2 ligands, the charge is delocalized over the AsF_6^- anion, giving it a net charge of −0.96 for the XeF_2 adduct and −0.95 for the KrF_2 adduct, close to the net charge of the free AsF_6^- anion. In both adducts, the anion is weakly coordinated, as demonstrated by the low Br−F_b bond orders of the XeF_2 and KrF_2 adducts (0.03 and 0.04, respectively). Overall, there is little effect on the anion when xenon is replaced by krypton. Thus, the dominant valence bond structures for $[BrOF_2][AsF_6]\cdot 2XeF_2$ are very similar to those of $[BrOF_2][AsF_6]\cdot 2KrF_2$[14] with the major contribution from structure V and a smaller contribution from structure VI.

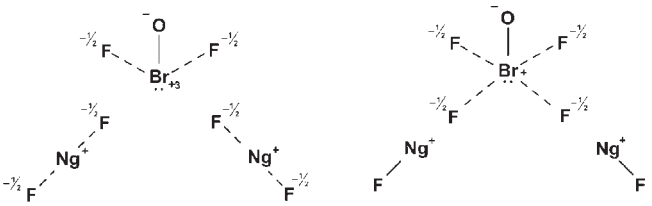

V VI

(c) QTAIM and ELF Analyses. The bonding was investigated by complementary use of the Quantum Theory of Atoms in Molecules (QTAIM)[53] and the topological analysis[54] of the Becke and Edgecombe Electron Localization Function (ELF).[55] For the ensuing discussion, the following abbreviations denote atomic populations, $\bar{N}$(A); electron localization function, $\eta(\mathbf{r})$; core basins, C(A); valence basins, V(A, B, ...); monosynaptic basins, V(A); disynaptic basins, V(A, B); and closed isosurfaces, $\eta(\mathbf{r}) = f$, where f is defined as the isosurface contour. The QTAIM and ELF analyses of the XeF_2 and $[BrOF_2][AsF_6]_3^{2-}$ fragments are provided in the Supporting Information.

Bonding in $[BrOF_2][AsF_6]\cdot 2XeF_2$. The QTAIM populations provide a charge transfer picture in which ca. 0.11 *e* is transferred from each XeF_2 and 0.05 *e* from AsF_6^- to $BrOF_2^+$. These transfers are almost equal to those calculated previously for the krypton analogue.[14]

In the molecular graph of the complex, the bromine center is linked to the two bridging fluorine atoms, F_3 and F_5, of the XeF_2 groups and to F_7, which belongs to the AsF_6^- unit. The values of the Laplacian of the electron density at the bond critical points are positive and decrease with the Br−F internuclear distances, i.e., 0.158 (BrF_3), 0.147 (BrF_5, 0.077 (BrF_7), and 0.015 (BrF_9). The delocalization indexes between bromine and the weakly bonded fluorine atoms show almost the same trends: δ(Br,F_3 = 0.26, δ(Br,F_5) = 0.24, δ(Br,F_7) = 0.12, δ(Br,F_9) = 0.02. The $\eta(\mathbf{r})$ = 0.75 localization domains of the complex are shown in Figure 8, whereas the hierarchy of the ELF basins is given in Scheme 1. Although the coordination of bromine has increased to six, the V(Br) ("valence electron lone pair on Br") basin remains in the complex while its $\eta(\mathbf{r})$ = 0.75 localization domain follows a trend in which it contracts across the series $BrOF_2^+$[14] > $[BrOF_2][AsF_6]_3^{2-}$ (Figure S6, Supporting Information) > $[BrOF_2][AsF_6]\cdot 2XeF_2$ (Figure 8) ≈ $[BrOF_2][AsF_6]\cdot 2KrF_2$[14] to accommodate their respective environments.

Although the bonding between the different components is very similar in the $[BrOF_2][AsF_6]\cdot 2XeF_2$ and $[BrOF_2][AsF_6]\cdot 2KrF_2$ complexes, there is a significant difference in the perturbation of the XeF_2 units relative to the KrF_2 units upon complexation. In $[BrOF_2][AsF_6]\cdot 2XeF_2$, the populations of the fluorine valence basins are almost equal and the covariance matrix elements of these populations with $\bar{N}$[V(Xe)] have a rather small difference. In the complex, the Xe−F bonds involved in the fluorine

(53) Bader, R. F. W. *Atoms in Molecules: A Quantum Theory*; Oxford University Press: Oxford, U. K., 1990.
(54) Silvi, B.; Savin, A. *Nature* **1994**, *371*, 683–686.
(55) Becke, A. D.; Edgecombe, K. E. *J. Chem. Phys.* **1990**, *92*, 5397–5403.

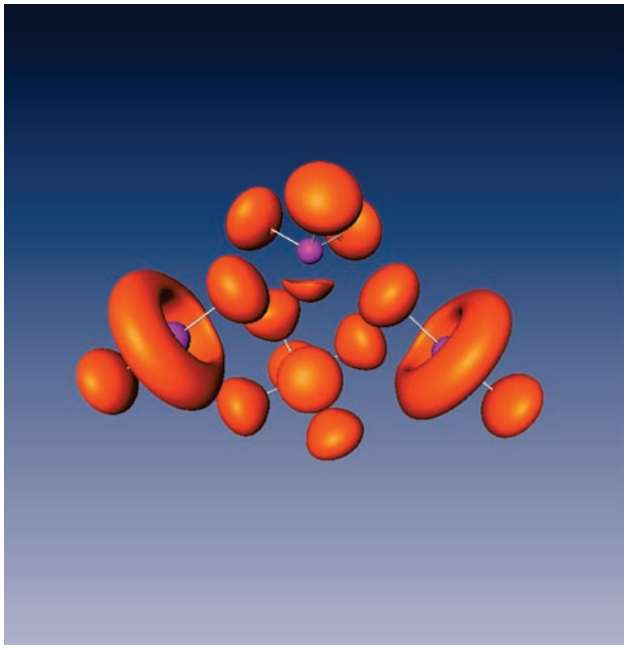

Figure 8. ELF localization domains for $[BrOF_2][AsF_6]\cdot 2XeF_2$. The isosurface value is $\eta(\mathbf{r}) = 0.75$. Color code: magenta = core, brick-red = monosynaptic basin.

Scheme 1. Reduction of Localization Diagram for $[BrOF_2][AsF_6]\cdot 2XeF_2$ Showing the Ordering of Localization Nodes and the Boundary Isosurface Value, $\eta(\mathbf{r})$, at which the Reducible Domains Split[a]

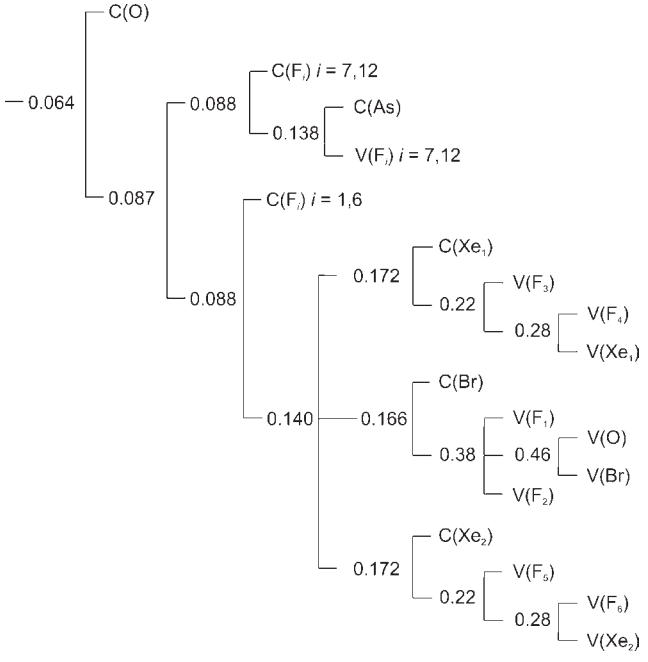

[a] The labeling scheme corresponds to that used in Figures 1 and 2.

bridges are more ionic than the Xe−F terminal bonds, in agreement with the respective lengthening and shortening of the corresponding internuclear distances relative to those of the uncomplexed species. In contrast, in the KrF_2 complex, there is a large contribution of the noble-gas atomic basin to the valence basin of the nonbridging fluorine atom, which correlates with the large increase of the absolute value of the covariance matrix element. The different behaviors of the two noble-gas atoms is likely due to the greater ionic character of the bonding in XeF_2.

Conclusion

The current study has demonstrated the propensity of the XOF_2^+ (X = Cl, Br) cations to attain pseudo-octahedral coordination spheres. The crystal structures of $[BrOF_2][AsF_6]$ and $[ClOF_2][AsF_6]$ have three fluorine-bridge contacts between the halogen atom of the cation and three nearest-neighbor AsF_6^- anions. In contrast, the $BrOF_2^+$ cation of $[BrOF_2][AsF_6]\cdot 2XeF_2$ forms only one fluorine bridge contact to the AsF_6^- anion and single fluorine bridges with each XeF_2 ligand. These structural features are reproduced in the calculated structures. Moreover, in the presence of HF at −78 °C, $[BrOF_2][AsF_6]\cdot XeF_2$ recombines to form $[BrOF_2][AsF_6]$ and $[BrOF_2][AsF_6]\cdot 2XeF_2$, thus attaining a Br(V) coordination number of six.

The X-ray crystal structure, vibrational spectrum, as well as the calculated structures and frequencies for $[BrOF_2][AsF_6]\cdot 2XeF_2$ are similar to those of the krypton analogue; however, notable differences occur. The contact distances between bromine and XeF_2 are shorter when compared with those of the KrF_2 analogue, consistent with the greater ionic character of the Xe−F bonds in XeF_2. The $\nu(XeF_t)$ modes of the XeF_2 strongly couple to one another, and the bridging modes only weakly couple to one another, whereas the opposite behavior is observed for $[BrOF_2][AsF_6]\cdot 2KrF_2$. The XeF_2 adduct undergoes internal fluoride ion abstraction at room temperature in HF solution forming $BrOF_3$ and $[Xe_2F_3][AsF_6]$. This contrasts with the KrF_2 adduct, which is stable in HF solution for at least 1 h at 20 °C. The latter behavior is again consistent with the greater ionic characters of the Ng−F bonds in XeF_2 when compared with those of KrF_2.

The ELF and QTAIM results indicate that the localization domain associated with the valence electron lone pair of bromine decreases across the series $BrOF_2^+ > [BrOF_2][AsF_6]_3^{2-} > [BrOF_2][AsF_6]\cdot 2XeF_2 \approx [BrOF_2][AsF_6]\cdot 2KrF_2$. The calculations also show that the covalencies of the $Kr-F_t$ bonds are significantly greater than those of the $Xe-F_t$ bond. In both adducts, the $Ng-F_t$ bonds are more covalent than their $Ng-F_b$ bonds.

Experimental Section

Apparatus and Materials. (a) General. All manipulations involving air-sensitive materials were carried out under strictly anhydrous conditions as previously described.[56] Reaction vessels/Raman sample tubes and NMR sample tubes were fabricated from ¼-in. o.d. and 4-mm o.d. FEP tubing, respectively, and outfitted with Kel-F valves. All reaction vessels and sample tubes were rigorously dried under a dynamic vacuum prior to passivation for at least 8 h with 1 atm of F_2 gas.

Xenon difluoride,[57] XeF_4,[58] $[ClOF_2][AsF_6]$,[33,39] and $[XeOTeF_5][AsF_6]$[59] were prepared and purified according to the literature methods. Anhydrous HF (Harshaw Chemicals Co.)[60] and BrF_5 (Matheson)[19] were purified by the standard literature methods.

(56) Casteel, W. J., Jr.; Dixon, D. A.; Mercier, H. P. A.; Schrobilgen, G. J. *Inorg. Chem.* **1996**, *35*, 4310–4322.
(57) Mercier, H. P. A.; Sanders, J. C. P.; Schrobilgen, G. J.; Tsai, S. S. *Inorg. Chem.* **1993**, *32*, 386–393.
(58) Chernick, C. L.; Malm, J. G. *Inorg. Synth.* **1966**, 254–258.
(59) Sladky, F. *Monatsh. Chem.* **1970**, *101*, 1578–1632.
(60) Emara, A. A. A.; Schrobilgen, G. J. *Inorg. Chem.* **1992**, *31*, 1323–1332.

High-purity Ar (99.998%, Air Liquide) or N_2 (obtained from liquid N_2 boil-off and dried by passage through a column of dry 3 Å molecular sieves) gases were used for backfilling vessels.

(b) $[BrOF_2][AsF_6]\cdot XeF_2$. In a typical synthesis, 70.5 mg (0.126 mmol) of $[XeOTeF_5][AsF_6]$ was added, inside a drybox, to a ¼-in. o.d. FEP reactor that was fitted to a Kel-F valve by means of a compression fitting. The solid was dissolved in ca. 0.3 mL of BrF_5 at −52 °C and warmed to room temperature as previously described.[13] The solution was cooled to −52 °C, and the solvent was immediately removed between −52 and −50 °C under a dynamic vacuum, leaving behind a white microcrystalline powder that contained adducted BrF_5. Completeness of solvent removal was monitored by Raman spectroscopy (Table S1, Supporting Information). The solid was pumped under a dynamic vacuum for 12 h with frequent agitation while maintaining the sample at −52 to −50 °C. This resulted in a fine white powder corresponding to $[BrOF_2][AsF_6]\cdot XeF_2$, which was shown by Raman spectroscopy to be free of coordinated BrF_5. The compound is stable indefinitely when stored under anhydrous conditions at −78 °C.

(c) $[BrOF_2][AsF_6]\cdot 2XeF_2$. In a typical synthesis, 45.6 mg (0.269 mmol) of XeF_2 was added, inside a drybox, to a ¼-in. o.d. FEP reactor containing 0.130 g (0.265 mmol) of $[BrOF_2][AsF_6]\cdot XeF_2$. The solids were dissolved in ca. 0.3 mL of aHF at −20 °C. Upon cooling the solution to −78 °C, a white microcrystalline powder, corresponding to $[BrOF_2][AsF_6]\cdot 2XeF_2$, precipitated from solution and was isolated by removal of the HF under a dynamic vacuum at −78 °C.

(d) $[BrOF_2][AsF_6]$. Crystals of $[BrOF_2][AsF_6]$ were isolated from a solution of $[BrOF_2][AsF_6]\cdot XeF_2$ in BrF_5 solvent (see Crystal Growth). In a typical synthesis, a 60.1 mg sample of $[BrOF_2][AsF_6]\cdot XeF_2$ was pumped under a dynamic vacuum for 20 h while maintaining the sample at 0 °C. This resulted in a fine, white powder corresponding to $[BrOF_2][AsF_6]$, which was shown to be free of coordinated XeF_2 by Raman spectroscopy. The compound is stable indefinitely when stored at −78 °C.

X-ray Crystallography. (a) Crystal Growth. Crystals of $[BrOF_2][AsF_6]\cdot 2XeF_2$ were grown as previously described[61] in a ¼-in. o.d. FEP T-shaped reaction vessel. A 124 mg (0.252 mmol) sample of $[BrOF_2][AsF_6]\cdot XeF_2$ was dissolved at ca. −18 °C in ca. 0.3 mL of HF. The solution was cooled from −28 to −32 °C over the course of 12 h, yielding crystals of $[BrOF_2][AsF_6]\cdot 2XeF_2$. When crystal growth was deemed complete, the reaction vessel was adjusted to and maintained at −35 °C, while the supernatant was decanted into the side arm of the reaction vessel, which was maintained at −78 °C. The side arm containing the supernatant was then cooled to −196 °C and heat-sealed under dynamic vacuum. The remaining crystals were dried under dynamic vacuum at −35 °C and stored at −78 °C until a suitable crystal could be selected and mounted on the X-ray diffractometer.

The attempted growth of $[BrOF_2][AsF_6]\cdot XeF_2$ crystals yielded crystalline $[BrOF_2][AsF_6]$ instead. A solution (0.1 mL) of BrF_5 containing 67.0 mg (0.136 mmol) $[BrOF_2][AsF_6]\cdot XeF_2$ was slowly pumped under a dynamic vacuum at −60 °C. Small, clear, needle-shaped crystals of $[BrOF_2][AsF_6]$ grew over a period of 2 h and were isolated by rapidly pumping the remaining solvent off under a dynamic vacuum at −35 °C. The crystals were stored at −78 °C until a suitable crystal could be selected and mounted on the X-ray diffractometer.

Attempts to grow crystals of a XeF_2 adduct with $[ClOF_2][AsF_6]$ resulted in the growth of $[ClOF_2][AsF_6]$ and $[Xe_2F_3][AsF_6]$ crystals instead. A ¼-in. o.d. FEP T-shaped reaction vessel containing 0.3 mL of HF, 33.2 mg (0.115 mmol) of $[ClOF_2][AsF_6]$, and 19.5 mg (0.122 mmol) of XeF_2 was warmed to ca. 25 °C in order to dissolve the solids. Slow cooling of the solution from −59 and −62 °C resulted in the formation of block-shaped crystals over the course of 4 h, which were found to be $[Xe_2F_3][AsF_6]$ (trigonal phase,[17] vide infra). When crystal growth was deemed complete, most of the supernatant (−62 °C) was decanted into the side arm of the reaction vessel (−78 °C), and the side arm was frozen at −196 °C and sealed off under a dynamic vacuum. When the residual solvent surrounding the $[Xe_2F_3][AsF_6]$ crystals was removed under a dynamic vacuum at −65 °C, numerous thin, brittle, plate-shaped crystals corresponding to $[ClOF_2][AsF_6]$ (vide infra) instantly grew in admixture with crystalline $[Xe_2F_3][AsF_6]$. The crystals were stored at −78 °C until suitable crystals could be selected and mounted on the diffractometer. The block-shaped crystals had a unit cell consistent with the trigonal phase of $[Xe_2F_3][AsF_6]$,[17] whereas the thin plates were shown to be $[ClOF_2][AsF_6]$.

(b) Crystal Mounting. The crystals were dumped into a trough cooled to −110 ±5 °C by a cold stream of dry N_2 gas, and individual crystals were selected from the bulk sample for mounting on a diffractometer as previously described.[62] Single crystals were mounted on glass fibers at −110 ±5 °C using a Fomblin oil as the adhesive. The crystals used for data collection were colorless and transparent and had the following dimensions: $[BrOF_2][AsF_6]\cdot 2XeF_2$, 0.20 × 0.20 × 0.18 mm; $[BrOF_2][AsF_6]$, 0.20 × 0.06 × 0.06 mm; and $[ClOF_2][AsF_6]$, 0.16 × 0.12 × 0.02 mm.

(c) Collection and Reduction of X-Ray Data. Single crystals were centered on a SMART APEX II diffractometer, equipped with an APEX II 4K charge-coupled device (CCD) area detector and a triple-axis goniometer, controlled by the APEX2 Graphical User Interface (GUI) software,[63] using graphite-monochromated Mo Kα radiation (λ = 0.71073 Å). The diffraction data collections consisted of a full ϕ rotation at fixed χ = 54.74° (using 1010) 0.36° frames, followed by a series of short (250 frames) ω scans at various ϕ settings to fill the gaps. The crystal-to-detector distance was 4.969 cm for $[BrOF_2][AsF_6]\cdot 2XeF_2$ and $[BrOF_2][AsF_6]$, and 4.982 cm for $[ClOF_2][AsF_6]$. The data collections were carried out in a 512 × 512 pixel mode using 2 × 2 pixel binning. Processing was carried out by using the APEX2 GUI software,[63] which applied Lorentz and polarization corrections to three-dimensionally integrated diffraction spots. The program SADABS[64] was used for scaling the diffraction data, the application of a decay correction, and an empirical absorption correction based on redundant reflections.

(d) Solution and Refinement of the Structures. The XPREP[65] program was used to confirm the unit cell dimensions and the crystal lattices. The $[BrOF_2][AsF_6]\cdot 2XeF_2$, $[BrOF_2][AsF_6]$, and $[ClOF_2][AsF_6]$ structures were solved in the space groups $P2_1/c$, $P2_13$, and $Pna2_1$, respectively, by use of direct methods, and the solutions yielded the positions of all the atoms. The final refinements were obtained by introducing anisotropic parameters for all the atoms, extinction parameters, and the recommended weight factors. The maximum electron densities in the final difference Fourier maps were located around the heavy atoms. A positional disorder arises for the $BrOF_2^+$ cation in $[BrOF_2][AsF_6]$ in which the oxygen and fluorine atoms could not be distinguished from one another. The PLATON program[66] could not suggest additional or alternative symmetries.

NMR Spectroscopy. (a) Instrumentation. Xenon-129 and ^{19}F NMR spectra were recorded unlocked (field drift < 0.1 Hz h^{-1}) on a Bruker DRX-500 spectrometer equipped with an 11.744-T cryomagnet. For low-temperature work, the NMR probe was cooled using a nitrogen flow and a BV-T 3000

(61) Lehmann, J. F.; Dixon, D. A.; Schrobilgen, G. J. *Inorg. Chem.* **2001**, *40*, 3002–3017.

(62) Gerken, M.; Dixon, D. A.; Schrobilgen, G. J. *Inorg. Chem.* **2000**, *39*, 4244–4255.

(63) *APEX2*, release 2.0−2; Bruker AXS Inc.: Madison, WI, 1995.

(64) Sheldrick, G. M. *SADABS* (*Siemens Area Detector Absorption Corrections*), version 2.03; Madison, WI, 1999.

(65) Sheldrick, G. M. *SHELXTL-Plus*, release 5.1; Siemens Analytical X-ray Instruments, Inc.: Madison, WI, 1998.

(66) Spek, A. L. *J. Appl. Crystallogr.* **2003**, *36*, 7–13.

variable-temperature controller. Fluorine-19 NMR spectra were acquired using a 5-mm combination $^{1}H/^{19}F$ probe operating at 470.593 MHz, and ^{129}Xe NMR spectra were obtained using a 5-mm broad-band inverse probe operating at 139.051 MHz. Spectra were recorded in 131K (^{19}F) and 32K (^{129}Xe) memories, with spectral width settings of 89 (^{19}F) and 97 (^{129}Xe) kHz, yielding data-point resolutions of 0.68 (^{19}F) and 2.96 (^{129}Xe) Hz/data point and acquisition times of 0.68 (^{19}F) and 0.17 (^{129}Xe) s. Pulse widths (μs), corresponding to bulk magnetization tip angles of approximately 90°, were 8.50 (^{19}F) and 10.0 (^{129}Xe). Relaxation delays of 0.10 (^{19}F) and 0.10 (^{129}Xe) s were applied, and 5000 (^{19}F) and 10 000 (^{129}Xe) transients were accumulated. Line broadenings of 0 (^{19}F) and 2 (^{129}Xe) Hz were used in the exponential multiplication of the free induction decays prior to Fourier transformation. The ^{19}F and ^{129}Xe spectra were referenced externally at 30 °C to samples of neat $CFCl_3$ and $XeOF_4$, respectively. The chemical shift convention used is that a positive (negative) sign indicates a chemical shift to high (low) frequency of the reference compound.

(b) NMR Sample Preparation. Sample tubes were fabricated by fusing 4-mm o.d. FEP tubing to short sections of ¼-in. o.d. × $^{1}/_{8}$-in. i.d. FEP tubing that were, in turn, joined to Kel-F valves by 45° SAE compression fittings. In these sample tubes, smaller amounts of $[BrOF_2][AsF_6]\cdot XeF_2$ (0.035 mmol) and $[BrOF_2][AsF_6]\cdot 2XeF_2$ (0.030 mmol) were prepared in the manner described above. Bromine pentafluoride was initially condensed onto the sample tube walls at −196 °C followed by melting onto the solid at −50 °C, to give a solvent depth of ca. 5 cm. The reactor was attached to a vacuum manifold, and the NMR sample tube was cooled to −196 °C and heat-sealed under a dynamic vacuum and stored at −78 °C until NMR spectra could be obtained. Samples were dissolved−just prior to data acquisition at or below the temperature used to record their spectra. The 4-mm o.d. FEP sample tubes were inserted into 5-mm o.d. thin wall precision glass NMR tubes (Wilmad) when spectra were recorded.

Raman Spectroscopy. Raman spectra were recorded on a Bruker RFS 100 FT-Raman spectrometer at −150 °C using 1064-nm excitation, 300 mW laser power, and 1 cm^{-1} resolution as previously described.[62]

Computational Results. The optimized geometries and frequencies of $[BrOF_2][AsF_6]_3^{2-}$, $[ClOF_2][AsF_6]_3^{2-}$, $[BrOF_2][AsF_6]\cdot XeF_2$, and $[BrOF_2][AsF_6]\cdot 2XeF_2$ were initially calculated at the B3LYP and PBE1PBE levels of theory using Stutt Huzpolar 2 basis sets[67] for $[BrOF_2][AsF_6]_3^{2-}$ and $[ClOF_2][AsF_6]_3^{2-}$; aug-cc-pVTZ for O and F and aug-cc-pVTZ-(PP) for Xe, As, and Br basis sets[67] for $[BrOF_2][AsF_6]\cdot XeF_2$; and $[BrOF_2][AsF_6]\cdot 2XeF_2$. The NBO analyses[49−52] were performed for the SVWN and MP2 optimized local minima. Quantum-chemical calculations were carried out using the program Gaussian 03[68] for geometry optimizations, vibrational frequencies, and their intensities. The program GaussView[69] was used to visualize the vibrational displacements that form the basis of the vibrational mode descriptions given in Tables 4−7 and Tables S4, S5, and S8 in the Supporting Information.

For all the systems studied, the all-electron wave functions have been calculated from the PBE1PBE/aug-cc-pVTZ(-PP) optimized geometries using the DGDZVP basis set.[70] In order to validate the use of this basis set in the topological analysis, the ELF populations and covariance matrix elements of the XeF_2 system were compared with those calculated at the PBE1PBE/aug-cc-pVTZ(-PP) and PBE1PBE/DGDZVP levels; the fluorine atomic basin population is larger by 0.03*e* for the pseudopotential calculation, in agreement with the ELF fluorine valence basin populations. The latter differ by the same amount, whereas the distributions of the core and valence populations of xenon differ slightly because the descriptions of the inner shells are not identical. The QTAIM and ELF calculations have been carried out with the TopMod package.[71,72] The ELF isosurfaces have been visualized with the Amira 3.0 software.[73]

Acknowledgment. We thank the Natural Sciences and Engineering Research Council of Canada for support in the form of a Discovery Grant (G.J.S.), the Ontario Graduate Scholarship in Science and Technology and the McMaster Internal Prestige "Ontario Graduate Fellowships" Programs for support (D.S.B.), and the computational resources provided by SHARCNet (Shared Hierarchical Academic Research Computing Network; www.sharcnet.ca).

Supporting Information Available: Experimental frequencies documenting removal of BrF_5 (Table S1); calculated geometry of $[ClOF_2][AsF_6]_3^{2-}$ (Figure S1); complete Tables 2 (Table S2) and 3 (Table S3); crystal packing diagram for $[ClOF_2][AsF_6]$ (Figure S2); complete Tables 4 (Table S4) and 5 (Table S5); calculated geometries of $[BrOF_2][AsF_6]_3^{2-}$ (Figure S3) and $[BrOF_2][AsF_6]\cdot XeF_2$ (Figure S4); factor-group analysis for $[BrOF_2][AsF_6]\cdot 2XeF_2$ (Table S6); factor-group analysis for $[ClOF_2][AsF_6]$ (Table S7); experimental and calculated vibrational frequencies for XeF_2 (Table S8); calculated geometrical parameters for $[BrOF_2][AsF_6]_3^{2-}$ (Table S9) and $[BrOF_2][AsF_6]\cdot XeF_2$ (Table S10); NBO valencies, bond orders, and NPA charges for $[BrOF_2][AsF_6]\cdot XeF_2$ (Table S11), $[ClOF_2][AsF_6]_3^{2-}$, and $[BrOF_2][AsF_6]_3^{2-}$ (Table S12) and $[BrOF_2][AsF_6]\cdot 2XeF_2$, $[BrOF_2][AsF_6]\cdot 2KrF_2$, and XeF_2 (Table S13); QTAIM and ELF analyses for XeF_2 and $[BrOF_2][AsF_6]_3^{2-}$; QTAIM atomic populations, delocalization indexes, ELF basin population and covariance matrix elements of the NgF_2 (Ng = Xe, Kr) molecules isolated and interacting with the bromine atom in the adducts (Table S14); ELF localization domains of XeF_2 (Figure S5) and $[BrOF_2][AsF_6]_3^{2-}$ (Figure S6); complete reference 68; and X-ray crystallographic files in CIF format for the structure determinations of $[BrOF_2][AsF_6]\cdot 2XeF_2$, $[BrOF_2][AsF_6]$, and $[ClOF_2][AsF_6]$. This information is available free of charge via the Internet at http://pubs.acs.org.

(67) Basis sets were obtained from the Extensible Computational Chemistry Environment Basis Set Database, version 2/25/04, as developed and distributed by the Molecular Science Computing Facility, Environmental and Molecular Science Laboratory, which is part of the Pacific Northwest Laboratory, P.O. Box 999, Richland, WA 99352.

(68) Frisch, M. J. et al. *Gaussian 98*, revision A.11; Gaussian, Inc.: Pittsburgh, PA, 2003.

(69) *GaussView*, release 3.0; Gaussian Inc.: Pittsburgh, PA, 2003.

(70) Godbout, N.; Salahub, D. R.; Andzelm, J.; Wimmer, E. *Can. J. Chem.* **1992**, *70*, 560–571.

(71) Noury, S.; Krokidis, X.; Fuster, F.; Silvi, B. *Comput. Chem.* **1999**, *23*, 597–604.

(72) Matito, E.; Silvi, B.; Duran, M.; Solà, M. *J. Chem. Phys.* **2006**, *125*, 024301.

(73) *Amira 3.0*; Template Graphics Software, Inc.: San Diego, CA, 2002.